

1 **Membrane lectins enhance SARS-CoV-2 infection and influence the**
2 **neutralizing activity of different classes of antibodies**

3

4 Florian A. Lempp¹, Leah Soriaga¹, Martin Montiel-Ruiz¹, Fabio Benigni², Julia Noack¹, Young-Jun
5 Park³, Siro Bianchi², Alexandra C. Walls³, John E. Bowen³, Jiayi Zhou¹, Hannah Kaiser¹, Maria
6 Agostini¹, Marcel Meury¹, Exequiel Dellota Jr.¹, Stefano Jaconi², Elisabetta Cameroni², Herbert W.
7 Virgin^{1,4,5}, Antonio Lanzavecchia², David Veessler³, Lisa Purcell⁶, Amalio Telenti^{1*}, Davide Corti^{2*}

8

9 *Equal contribution

10 ¹Vir Biotechnology, San Francisco, CA 94158, USA.

11 ²Humabs Biomed SA, a subsidiary of Vir Biotechnology, 6500 Bellinzona, Switzerland.

12 ³Department of Biochemistry, University of Washington, Seattle, WA 98195, USA

13 ⁴Department of Pathology and Immunology, Washington University School of Medicine, Saint Louis MO 63110,
14 USA

15 ⁵Department of Internal Medicine, UT Southwestern Medical Center, Dallas, TX 75390, USA

16 ⁶Vir Biotechnology, St Louis, MO, 63110, USA.

17

18

19 **Correspondence:** atelenti@vir.bio, dcorti@vir.bio

20

21 **Key words:** SARS-CoV-2; COVID-19; antibody, vaccine, neutralising antibodies; mutation; lectin
22 **receptors, auxiliary-receptors, sialic acid.**

23

24 **Abstract**

25 **Investigating the mechanisms of SARS-CoV-2 cellular infection is key to better**
26 **understand COVID-19 immunity and pathogenesis. Infection, which involves both cell**
27 **attachment and membrane fusion, relies on the ACE2 receptor that is paradoxically**
28 **found at low levels in the respiratory tract, suggesting that additional mechanisms**
29 **facilitating infection may exist. Here we show that C-type lectin receptors, DC-SIGN, L-**
30 **SIGN and the sialic acid-binding Ig-like lectin 1 (SIGLEC1) function as**
31 **auxiliary receptors by enhancing ACE2-mediated infection and modulating the**
32 **neutralizing activity of different classes of spike-specific antibodies. Antibodies to the N-**
33 **terminal domain (NTD) or to the conserved proteoglycan site at the base of the Receptor**
34 **Binding Domain (RBD), while poorly neutralizing infection of ACE2 over-expressing**
35 **cells, effectively block lectin-facilitated infection. Conversely, antibodies to the Receptor**
36 **Binding Motif (RBM), while potently neutralizing infection of ACE2 over-expressing**
37 **cells, poorly neutralize infection of cells expressing DC-SIGN or L-SIGN and trigger**
38 **fusogenic rearrangement of the spike promoting cell-to-cell fusion. Collectively, these**
39 **findings identify a lectin-dependent pathway that enhances ACE2-dependent infection by**
40 **SARS-CoV-2 and reveal distinct mechanisms of neutralization by different classes of**
41 **spike-specific antibodies.**

42

43 **Introduction**

44

45 SARS-CoV-2 infects target cells via the spike glycoprotein (S) that is organized as a
46 homotrimer wherein each monomer is comprised of S1 and S2 subunits^{1,2}. The infectious
47 process includes binding to cells, triggering of S conformational changes and then fusion of the
48 viral envelope with the target cell membrane. The S1 subunit comprises the N-terminal domain
49 (NTD) and the receptor binding domain (RBD), the latter interacting with ACE2 through a
50 region defined as the receptor binding motif (RBM). Antibodies against the RBD contribute to
51 the majority of the neutralizing activity in polyclonal serum antibodies^{3,4}, potently neutralize
52 SARS-CoV-2 in vitro^{5,6} and have shown efficacy in clinical trials for prophylaxis and early
53 therapy of COVID-19^{7,8}.

54 The search for SARS-CoV-2 neutralizing antibodies has been facilitated by the use of
55 target cells over-expressing the ACE2 receptor⁹. However, while ACE2 is highly expressed in
56 several tissues including the intestine and kidney, its expression in the respiratory tract is
57 limited, with low levels found in only a limited number of type-II alveolar basal, goblet and
58 mucous cells¹⁰⁻¹². The paradox of low ACE2 levels in the lung and infection in other tissues
59 leading to extrapulmonary complications¹³, raises the possibility that additional receptors may
60 contribute to viral infection and dissemination, such as DC-SIGN (CD209), L-SIGN
61 (CD209L/CLEC4M), neuropilin-1 (NRP-1), basigin (CD147) and heparan sulfate¹⁴⁻¹⁸. It

62 remains to be established whether these molecules may act as alternative receptors for viral
63 entry, as co-receptors or as auxiliary receptors that tether viral particles enhancing their
64 interaction with ACE2.

65 In this study, we identify DC-SIGN, L-SIGN and SIGLEC1 as auxiliary receptors that
66 enhance ACE2-dependent infection and demonstrate different mechanisms of neutralization by
67 antibodies targeting RBM and non-RBM sites in the presence or absence of lectins.

68 69 **Results**

71 **DC-SIGN, L-SIGN and SIGLEC1 act as auxiliary receptors for ACE2-dependent SARS-** 72 **CoV-2 infection**

73 To develop an assay for identification of accessory receptors of SARS-CoV-2 infection, we
74 took advantage of HEK293T cells that express low endogenous levels of ACE2. HEK293T
75 were transfected with vectors encoding ACE2 or 13 selected lectins and published receptor
76 candidates prior to infection with VSV-SARS-CoV-2. As expected, untransfected HEK293T
77 cells were only weakly permissive to infection, and ACE2 overexpression led to a dramatic
78 increased pseudovirus entry. Interestingly, increased infectivity was also observed in
79 HEK293T cells following transfection with C-type lectins DC-SIGN and L-SIGN that were
80 previously reported as entry receptors^{14,15,19}, as well as with SIGLEC1, which was not
81 previously shown to mediate SARS-CoV-2 entry (**Fig. 1a**). In contrast, NRP-1 and CD147 did
82 not enhance SARS-CoV-2 infection in these conditions although they were previously
83 suggested to act as entry receptors^{16,17}. The infection-enhancing activity of the three lectins was
84 also observed with authentic SARS-CoV-2 and stably transduced HEK293T cells (**Fig. 1b-c**
85 and **Extended Data Fig. 1**). A SIGLEC1 blocking antibody inhibited in a dose-dependent
86 fashion the infection of SIGLEC1 expressing HEK293T, supporting the role of this molecule
87 as a new SARS-CoV-2 entry factor (**Fig. 1d**).

88 The ectopic expression of DC-SIGN, L-SIGN and SIGLEC1 did not support infection
89 of ACE2 negative cells, such as HeLa or MRC-5 cells (**Fig. 1e**), indicating that these lectins
90 do not act as entry receptors. The requirement of ACE2 for viral infection of lectin-expressing
91 cells was also demonstrated using ACE2 blocking antibodies or ACE2-siRNA (**Fig. 1f-g**). Of
92 note, the B.1.1.7 UK variant of concern (VOC) which is currently the most prevalent
93 circulating virus in Europe retained the capacity to use DC-SIGN, L-SIGN and SIGLEC1 as
94 auxiliary receptors (**Extended Data Fig. 1c**).

95 Collectively, these data reveal a lectin-facilitated pathway of infection that is evident
96 on cells expressing low levels of ACE2, supporting the notion that SARS-CoV-2 may use these
97 lectins as auxiliary receptors for ACE2-mediated entry.

98

99 **Auxiliary receptors can facilitate trans-infection of ACE2⁺ cells**

100 The above data suggest that lectin receptors may act as auxiliary receptors that tether
101 viral particles to the cell membrane facilitating interaction with ACE2. This could take place
102 in *cis* (on the same cell) or in *trans* effectively promoting cell-to-cell trans-infection, as
103 reported for HIV-1²⁰. To address whether ACE2 and lectins can be found on the same cells,
104 we interrogated the lung cell atlas²¹ and identified the cell types that express these receptors
105 (**Fig. 2a**). DC-SIGN (CD209) is expressed most prominently on IGSF21⁺ dendritic cells, L-
106 SIGN (CLEC4M; CD209L) has a limited expression on vascular structures and SIGLEC1
107 (CD169) is broadly expressed at the surface of alveolar macrophages, dendritic cells and
108 monocytes. As previously noted, ACE2 expression is limited to subsets of alveolar epithelial
109 type-2, basal and goblet cells. Next, we mined the recently released single-cell transcriptomics
110 data on 3,085 lung epithelial and immune cells obtained from bronchoalveolar lavage fluid or
111 sputum of 8 individuals that suffered from severe COVID-19²². The distribution of viral RNA
112 per cell, expressed as log counts per million (logCPM), varied across annotated cell types.
113 Specifically, the content of viral RNA in macrophages is greater relative to secretory cells (2-
114 sided K-S statistic and p-value, D = 0.32092, p-value < 2.2e-16) (**Fig. 2b**). SIGLEC1 was
115 expressed in 41.4% (459/1107 cells) of SARS-CoV-2⁺ macrophages, whereas ACE2
116 expression was negligible in these cells (**Fig. 2c**). Conversely, ACE2 expression was found in
117 10.6% (60/565 cells) of SARS-CoV-2⁺ secretory cells, whereas SIGLEC1 expression was
118 negligible (**Fig. 2c**). Plotting SIGLEC1, DC-SIGN and L-SIGN expression as a function of
119 SARS-CoV-2 viral load revealed a strong positive correlation for SIGLEC1 in macrophages
120 (**Fig. 2c**). We confirmed this association in a separate transcriptomics dataset of 1,072 SARS-
121 CoV-2⁺ bronchoalveolar lavage fluid cells from individuals with severe COVID-19²³. We
122 inspected the available sequenced reads from this dataset to assess the nature of viral RNA in
123 SARS-CoV-2⁺ bronchoalveolar lavage cells. Reads which supported a junction between the 5'
124 leader sequence and the transcription regulatory sequence (TRS) preceding open reading
125 frames for viral genes were counted as evidence of subgenomic mRNA, a surrogate readout
126 for viral replication. Such reads constituted a small fraction of TRS-containing viral reads,

127 ranging from undetectable to 3.4%, suggesting that minimal replication was occurring in this
128 cell population largely comprised of macrophages and other non-epithelial cell types.

129 The above results suggest limited cooperation of ACE2 and SIGLEC1 in *cis* because
130 these receptors are rarely expressed in the same cell. However, the data support the possibility
131 of *trans*-infection from SIGLEC1⁺ macrophages to ACE2⁺ cells. To test this hypothesis, we
132 developed an in vitro model where single-round VSV-SARS-CoV-2 was adsorbed on ACE2-
133 negative HeLa cells either untransduced or transduced with DC-SIGN, L-SIGN or SIGLEC1.
134 Under these conditions, lectin-transduced HeLa cells showed enhanced capacity to promote
135 VSV-SARS-CoV-2 *trans*-infection of susceptible Vero-E6-TMPRSS2 target cells (**Fig. 2d**),
136 and SIGLEC1-mediated *trans*-infection was inhibited by SIGLEC1-blocking antibodies (**Fig.**
137 **2e**). Collectively, these results are consistent with the possible role of lectins in the
138 enhancement of ACE2-mediated *trans*-infection leading to dissemination of SARS-CoV-2.

139

140 **Over-expression of ACE2 reduces neutralization of SARS-CoV-2 by mAbs that do not** 141 **block ACE2 attachment**

142 Cell line selection and the level of ACE2 expression are important variables in
143 assessing the potency of SARS-CoV-2 neutralizing mAbs. Previous studies suggested that non-
144 RBM mAbs, such as S309 (parent of the clinical stage VIR-7831 antibody) and NTD-specific
145 mAbs showed a reduced and partial neutralizing activity when using target cells over-
146 expressing ACE2²⁴⁻²⁶.

147 To further investigate how ACE2 and auxiliary receptor expression levels influence
148 neutralizing activity, we compared three mAbs targeting distinct sites on the spike protein: i)
149 S2E12, targeting the RBM site Ia/class 1 on RBD⁵; ii) S309 targeting the conserved
150 proteoglycan site IV/class 3 distal from RBM²⁷ and iii) S2X333, targeting site i on NTD²⁸ (**Fig.**
151 **3a**). These mAbs completely neutralize infection of Vero E6 cells with authentic SARS-CoV-
152 2, albeit with different potencies, and their activity was not influenced by the expression of the
153 TMPRSS2 protease (**Fig. 3b-c and Extended Data Fig. 2a**). To understand the influence of
154 receptor expression on neutralization, we used cell lines expressing ACE2 and TMPRSS2
155 (endogenously or upon transduction) at levels varying more than 1000-fold as evaluated by
156 qPCR and by flow cytometry staining with RBD or S proteins (**Fig. 3d-e and Extended Data**
157 **Fig. 2b**). Whereas the RBM mAb, S2E12 showed comparable neutralizing activity on all target
158 cells, both S309 and S2X333 showed an impaired neutralizing activity when tested on cells

159 over-expressing ACE2, both in terms of maximal neutralization and potency (**Fig. 3f-g** and
160 **Extended Data Fig. 2c**). This observation was particularly evident for S309 and S2X333 when
161 tested on HEK293T cells over-expressing ACE2. Comparable results were obtained with both
162 VSV-SARS-CoV-2 and authentic SARS-CoV-2-Nluc. Overall, a negative correlation was
163 found between ACE2 levels and neutralization potency for non-RBM mAbs (**Extended Data**
164 **Fig. 2c**).

165 These results demonstrate that the potency of neutralizing mAbs targeting epitopes
166 outside the RBM negatively correlates with ACE2 expression levels on target cells.
167 Consequently, the widespread use of ACE2-overexpressing cells leads to underestimation of
168 the neutralizing activity of non-RBM antibodies, which is well-detected when using cells
169 expressing moderate to low levels of ACE2, possibly corresponding to the physiological ACE2
170 expression levels.

171 Given the uncertainty on the most relevant *in vitro* correlates of protection, we
172 investigated the capacity of hamsterized S309 and S2E12 mAbs to prevent SARS-CoV-2
173 infection in Syrian hamsters, a relevant animal model that relies on endogenous expression of
174 ACE2²⁹. In a prophylactic setting, S309 was highly effective at doses as low as 0.4 mg/kg in
175 terms of reduction of viral RNA and infectious virus levels and histopathological score in the
176 lungs (**Extended Data Fig. 3a**). Furthermore, we did not observe substantial increased efficacy
177 by co-administering S309 with an equal amount of the potent RBM S2E12 mAb (**Extended**
178 **Data Fig. 3b**). This result is reminiscent of the lack of increased efficacy observed in an early
179 therapy clinical trial where the combination of bamlanivimab and etesevimab mAbs was
180 compared to bamlanivimab alone³⁰.

181 Since S309 induces potent Fc-mediated effector functions *in vitro*²⁷, we set out to
182 determine their contribution *in vivo* using the hamster model. The S309 mAb harboring the Fc
183 null N297A mutation on the hamster IgG2 Fc failed to bind to hamster monocytes (**Extended**
184 **Data Fig. 4**), indicating an expected lack of activation of effector functions *in vivo*. This ‘Fc-
185 silenced’ S309 mAb, however, was similarly protective as wildtype S309 against SARS-CoV-
186 2 challenge of hamsters underscoring that the neutralizing activity of S309 was the primary
187 mechanism of action in this condition (**Extended Data Fig. 5**), which is consistent with the
188 previous finding that in a prophylactic setting in hamsters viral neutralization is the primary
189 mode of action³¹.

190 Taken together, these data indicate that neutralization assays using cells over-expressing
191 ACE2 under-estimate the neutralizing activity of non-RBM mAbs, which are comparably
192 protective to RBM mAbs in a relevant animal model of infection^{32,33}. The significance of this
193 finding is also supported by the recent efficacy data of VIR-7831 in a Phase 3 clinical trial
194 demonstrating 85% protection against hospitalization and death due to COVID-19 in an interim
195 analysis.

196

197 **MAb-mediated conformational selection of open RBDs promotes membrane fusion**

198 Infection of permissive cells involves both interactions with ACE2 and auxiliary
199 receptors, as well as fusion of the viral membrane to cellular membranes. Here we investigated
200 how different classes of spike-specific antibodies may interfere with viral fusion events that are
201 involved in viral entry, but also in cell-to-cell fusion, leading to the formation of syncytia in
202 vitro³⁴ and of multi nucleate giant cells in human lung from infected individuals³⁵. We
203 previously showed that RBM-specific SARS-CoV neutralizing mAbs can act as ACE2 mimics
204 triggering the fusogenic rearrangement of the S protein³⁶. We evaluated mAbs of different
205 epitope specificity (**Extended Data Table 1**) to induce fusogenic rearrangement of soluble S
206 trimers as measured by negative stain electron microscopy imaging (**Fig. 4a**). Three RBM
207 mAbs (S2E12, S2X58, and S2D106) triggered rearrangement to the postfusion state of a native
208 SARS-CoV-2 S ectodomain trimer, likely due to conformational selection for open RBDs.
209 S2E12 and S2X58 triggered a rapid rearrangement of S, whereas S2D106 did so more slowly.
210 As expected, another RBM mAb (S2M11) that locks neighbouring RBDs in a closed state⁵ did
211 not induce fusogenic S rearrangements. Antibodies to NTD (S2X333) and to the proteoglycan
212 site at the base of RBD (S309) also did not trigger rearrangement due to the absence of
213 conformational selection for open RBDs.

214 To investigate whether the antibody-mediated triggering of fusogenic rearrangement
215 could promote membrane fusion, we evaluated a panel of mAbs for their capacity to induce
216 cell-cell fusion of CHO cells (lacking ACE2 expression) stably transduced with full-length
217 SARS-CoV-2 S (**Fig. 4b**). Syncytia formation was triggered by all mAbs recognizing antigenic
218 sites Ia and IIa (**Extended Data Table 1**), that are only accessible in the open RBD state, with
219 EC₅₀ values ranging from 20 ng/ml for S2E12 to >1 µg/ml for S2D106 (**Fig. 4c-d**). Syncytia
220 were also formed by the three clinical-stage mAbs REGN10933 (casirivimab), Ly-CoV016

221 (etesevimab) and CT-P59 (regdanvimab). In contrast, syncytia were not formed in the presence
222 of mAbs binding to the open and closed RBD states (S2M11, S309, bamlanivimab and
223 imdevimab), to the NTD (S2X333) and to a conserved site in the S2 subunit stem helix (S2P6).
224 An interesting exception is provided by S2X58, a mAb that was structurally defined in this
225 study as binding to the site Ib, which is accessible on open and closed RBDs (**Extended Data**
226 **Fig. 6**). However, due to steric clashes between the S2X58 Fab and the NTD of a neighboring
227 monomer in the closed S state, this mAb appears to conformationally select the open RBDs,
228 thus explaining its fusogenic activity. With regard to the possible interaction between fusogenic
229 and non-fusogenic antibodies, we found that syncytia formation induced by S2E12 could be
230 inhibited by different classes of antibodies comprising S2M11 (that locks RBDs in a closed
231 state), S309 (targeting a proteoglycan site at the base of RBD) and S2P6 (destabilizing the stem
232 helix in S2) (**Fig. 4e**). These results highlight that different combinations of antibodies may
233 interfere with each other by promoting or inhibiting membrane fusion.

234 To address if antibodies may promote cell-to-cell spread of the infection, we co-cultured
235 S-positive CHO cells with S-negative fluorescently labelled CHO cells. In these conditions
236 S2E12 mAb promoted unidirectional fusion of S-positive CHO cells with S-negative CHO cells
237 in the absence of ACE2 (defined here as “trans-fusion”) (**Fig. 4f**). To address if this mechanism
238 may also mediate ACE2 independent infection of tethered virus, we infected HeLa-DC-SIGN
239 cells with live SARS-CoV-2-Nluc virus in the presence of fusion-enhancing mAbs at different
240 dilutions. In these conditions S2E12, S2D106 and S2X58 failed to promote infection
241 (**Extended Data Fig. 7**). Collectively, these findings indicate that in certain conditions of
242 antibody concentration and cell-to-cell proximity a sub-class of RBM antibodies that select the
243 open conformation of RBD may promote cell-to-cell fusion with ACE2-negative cells.
244 However, the fusogenic activity of these mAbs may not be sufficient to promote entry of virions
245 tethered to the cell surface in the absence of ACE2. It remains to be established whether under
246 other conditions RBM mAbs may mediate ACE2-independent SARS-CoV-2 entry, as
247 previously observed for anti-MERS-CoV neutralizing mAbs captured by FcγRIIIa expressing
248 cells *in vitro*³⁷.

249

250 **Membrane lectin receptors modulate neutralizing activity by different classes of**
251 **antibodies**

252 Given the dual function of certain RBM antibodies in inhibiting ACE2 binding and
253 triggering fusion, and the dependence on auxiliary receptor expression of neutralization by
254 specific antibodies, we compared the neutralizing activity of a panel of mAbs using authentic
255 SARS-CoV-2 and target cells expressing different levels of ACE2 and lectin receptors. When
256 tested on cells over-expressing ACE2, all anti-RBM mAbs (S2E12, S2D106, S2X58 and
257 S2M11) potently neutralized infection, while non-RBM mAbs S309 and S2X333 failed to do
258 so (**Fig. 2** and **Fig. 5a**). However, when tested on cells expressing low levels of ACE2 together
259 with SIGLEC1, DC-SIGN or L-SIGN, S309 and S2X333 showed enhanced neutralizing
260 activity, with S309 reaching 100% of neutralization (**Fig. 5b-d** and **Extended Data Fig. 8**).
261 Intriguingly, while all RBM mAbs retained neutralizing activity on SIGLEC1⁺ cells, two of the
262 RBM mAbs (S2D106 and S2X58) lost neutralizing activity on cells expressing DC-SIGN or L-
263 SIGN showing only partial neutralization at the highest concentrations tested. Of note, the
264 S2E12 RBM mAb retained substantial neutralizing activity on lectin expressing cells. The only
265 RBM mAb that retained potent neutralizing activity on all target cells was S2M11, consistent
266 with its capacity to lock the RBDs in the closed state⁵, thereby preventing access of RBM-
267 specific antibodies to their cognate epitope. The loss of neutralizing activity of S2X58 and
268 S2D106 mAbs observed on DC-SIGN and L-SIGN expressing cells was confirmed with both
269 live SARS-CoV-2 (wildtype), as well as with live SARS-CoV-2-Nluc (**Extended Data Fig. 8**).
270 Collectively these data show that mAbs that do not block ACE2 attachment, such as S309 or
271 S2X333, potently neutralize ACE2-dependent, lectin-facilitated infection of target cells,
272 highlighting that they may act by inhibiting steps in viral binding and entry independent on the
273 interaction between the RBM and ACE2 (**Fig. 5e**).

274

275 **Discussion**

276 We have shown that transmembrane lectins act as auxiliary receptors, rather than entry
277 receptors for SARS-CoV-2^{14,15}, thus facilitating the infection via the canonical ACE2 pathway.
278 This finding likely addresses the efficiency of lower respiratory tract infection despite the
279 paradoxically low level of ACE2 expression, even in the presence of interferon^{38,39} which
280 induces the production of an ACE2 isoform that does not bind to SARS-CoV-2^{S40,41}. The
281 auxiliary role of lectins in SARS-CoV-2 infection is in line with the known biology of these
282 adhesion molecules that bind glycans characteristic of cellular membranes and pathogen
283 surfaces to promote trans-infection⁴². Among the three auxiliary receptors, SIGLEC1 is of

284 particular relevance because this receptor is prominently expressed in alveolar macrophages in
285 association with viral RNA, thus supporting a model of trans-infection, tissue dissemination
286 and the triggering of immune responses by myeloid cells, rather than a direct target for
287 productive infection⁴³. DC-SIGN and L-SIGN association with SARS-CoV-2 is also of
288 relevance because of their interaction with blood endothelium and role in immune activation.

289 Expression of lectin receptors can also influence the neutralizing activity of different
290 classes of spike-specific monoclonal antibodies, In addition, the present work identifies the
291 the ability of various mAbs to interfere with fusion events. We expand our initial observation
292 on SARS-CoV and MERS-CoV^{36,37} by showing that most RBM mAbs can trigger the fusogenic
293 rearrangement of S, albeit with varying efficiency. By stabilizing the RBDs in the open
294 conformations, these antibodies might act as receptor mimics. This finding suggests that
295 premature conformational triggering resulting in loss of the potential of a spike protein to
296 engender productive infection - we term this mechanism spike inactivation herein - may be the
297 prominent mode of viral neutralization for this class of antibodies, over the simple inhibition of
298 receptor binding. However, we have also shown that these antibodies can promote fusion of
299 Spike-expressing cells with neighboring cells, even if the latter lack ACE2. Intriguingly, the
300 formation of syncytia has been observed in autopsy samples from severe COVID-19 cases^{35,44-}
301 ⁴⁶. It is tempting to speculate that fusogenic antibodies although highly effective in preventing
302 and controlling the early phases of infection^{7,8,47}, may contribute at a later stage to the spread
303 of infection and inflammation.

304 Overall, our study highlights the novel finding that ranking of SARS-CoV-2 neutralizing
305 antibodies is highly dependent on the level of ACE2 expression and on the presence of auxiliary
306 receptors and identifies a mechanism that might possibly result in creation of multinucleate
307 viral factories potentially enhanced by specific antibodies. Such antibodies can be protective in
308 vivo regardless of the capacity to trigger, but this protective capacity may represent a balance
309 between neutralization and induction of fusion between infected cells in vivo. Our results
310 suggest that assessment of both vaccines and mAbs needs to include their effects on steps in
311 viral infection identified in this study.

312

313

314

315

316 **Acknowledgements**

317 We thank Nuria Izquierdo-Useros and Javier Martinez-Picado for useful commentary.

318

319 **Author contributions**

320 Conceived study: F.A.L., L.S., A.L., L.P., D.V., A.T. and D.C. Designed study and
321 experiments: F.A.L., L.S., F.B. and D.C. Performed in vitro virological experiments: F.A.L.,
322 F.B., Y-J.P., S.B., M.M-R., J.N., A.C.W., J.E.B., J.Z., H.K, M.A. EM data collection and
323 analysis: Y-J.P., A.C.W., J.E.B. Produced antibodies for in vitro and in vivo studies: S.J. and
324 E.C. Recombinant glycoprotein production: J.E.B., M.M., E.D. Hamster model and data
325 analysis: F.B. Bioinformatic analysis: L.S., A.T. Manuscript writing: F.A.L, F.B., L.P., D.V.,
326 A.L., A.T. and D.C. Supervision: L.P., D.V., H.W.V, A.T. and D.C.

327 **Competing interests**

328 F.A.L, L.S., F.B., S.B., M.M-R., J.N., J.Z, H.K., M.A., M.M., E.D., S.J., E.C., H.W.V., A.L.,
329 L.P, A.T. and D.C. are employees of Vir Biotechnology and may hold shares in Vir
330 Biotechnology. H.W.V. is a founder of PierianDx and Casma Therapeutics. L.P. is a former
331 employee and shareholder in Regeneron Pharmaceuticals. Neither company provided funding
332 for this work or is performing related work. D.V. is a consultant for Vir Biotechnology Inc.
333 The Veesler laboratory has received a sponsored research agreement from Vir Biotechnology
334 Inc. The remaining authors declare that the research was conducted in the absence of any
335 commercial or financial relationships that could be construed as a potential conflict of interest.

336 MATERIALS AND METHODS

337

338 *Generation of stable overexpression cell lines*

339 Lentiviruses were generated by co-transfection of Lenti-X 293T cells (Takara) with lentiviral
340 expression plasmids encoding DC-SIGN (CD209), L-SIGN (CLEC4M), SIGLEC1, TMPRSS2
341 or ACE2 (all obtained from Genecopoeia) and the respective lentiviral helper plasmids. Forty-
342 eight hours post transfection, lentivirus in the supernatant was harvested and concentrated by
343 ultracentrifugation for 2 h at 20,000 rpm. Lenti-X 293T (Takara), Vero E6 (ATCC), MRC5
344 (Sigma-Aldrich), A549 (ATCC) or HeLa (ATCC) cells were transduced in the presence of 6
345 ug/mL polybrene (Millipore) for 24 h. Cell lines overexpressing two transgenes were
346 transduced subsequently. Selection with puromycin and/or blasticidin (Gibco) was started two
347 days after transduction and selection reagent was kept in the growth medium for all subsequent
348 culturing. Single cell clones were derived from the A549-ACE2-TMPRSS2 cell line, all other
349 cell lines represent cell pools.

350

351 *SARS-CoV-2 neutralization*

352 Cells cultured in DMEM supplemented with 10% FBS (VWR) and 1x Penicillin/Streptomycin
353 (Thermo Fisher Scientific) were seeded in black 96-well plates at 20,000 cells/well. Serial 1:4
354 dilutions of the monoclonal antibodies were incubated with 200 pfu of SARS-CoV-2 (isolate
355 USA-WA1/2020, passage 3, passaged in Vero E6 cells) for 30 min at 37°C in a BSL-3 facility.
356 Cell supernatant was removed and the virus-antibody mixture was added to the cells. 24 h post
357 infection, cells were fixed with 4% paraformaldehyde for 30 min, followed by two PBS (pH
358 7.4) washes and permeabilization with 0.25% Triton X-100 in PBS for 30 min. After blocking
359 in 5% milk powder/PBS for 30 min, cells were incubated with a primary antibody targeting
360 SARS-CoV-2 nucleocapsid protein (Sino Biological, cat. 40143-R001) at a 1:2000 dilution for
361 1h. After washing and incubation with a secondary Alexa647-labeled antibody mixed with 1
362 ug/ml Hoechst33342 for 1 hour, plates were imaged on an automated cell-imaging reader
363 (Cytation 5, Biotek) and nucleocapsid-positive cells were counted using the manufacturer's
364 supplied software.

365

366 *SARS-CoV-2-Nluc neutralization*

367 Neutralization was determined using SARS-CoV-2-Nluc, an infectious clone of SARS-CoV-2
368 (based on strain 2019-nCoV/USA_WA1/2020) encoding nanoluciferase in place of the viral
369 ORF7, which demonstrates comparable growth kinetics to wild type virus (Xie et al., Nat

370 Comm, 2020, <https://doi.org/10.1038/s41467-020-19055-7>). Cells were seeded into black-
371 walled, clear-bottom 96-well plates at 20,000 cells/well (293T cells were seeded into poly-L-
372 lysine-coated wells at 35,000 cells/well) and cultured overnight at 37°C. The next day, 9-point
373 4-fold serial dilutions of antibodies were prepared in infection media (DMEM + 10% FBS).
374 SARS-CoV-2-Nluc was diluted in infection media at the indicated MOI, added to the antibody
375 dilutions and incubated for 30 min at 37°C. Media was removed from the cells, mAb-virus
376 complexes were added, and cells were incubated at 37°C for 24 h. Media was removed from
377 the cells, Nano-Glo luciferase substrate (Promega) was added according to the manufacturer's
378 recommendations, incubated for 10 min at RT and luciferase signal was quantified on a
379 VICTOR Nivo plate reader (Perkin Elmer).

380

381 *SARS-CoV-2 pseudotyped VSV production and neutralization*

382 To generate SARS-CoV-2 pseudotyped vesicular stomatitis virus, Lenti-X 293T cells (Takara)
383 were seeded in 10-cm dishes for 80% next day confluency. The next day, cells were transfected
384 with a plasmid encoding for SARS-CoV-2 S-glycoprotein (YP_009724390.1) harboring a C-
385 terminal 19 aa truncation using TransIT-Lenti (Mirus Bio) according to the manufacturer's
386 instructions. One day post-transfection, cells were infected with VSV(G*ΔG-luciferase)
387 (Kerafast) at an MOI of 3 infectious units/cell. Viral inoculum was washed off after one hour
388 and cells were incubated for another day at 37°C. The cell supernatant containing SARS-CoV-
389 2 pseudotyped VSV was collected at day 2 post-transfection, centrifuged at 1000 x g for 5
390 minutes to remove cellular debris, aliquoted, and frozen at -80°C.

391 For viral neutralization, cells were seeded into black-walled, clear-bottom 96-well plates at
392 20,000 cells/well (293T cells were seeded into poly-L-lysine-coated wells at 35,000 cells/well)
393 and cultured overnight at 37°C. The next day, 9-point 4-fold serial dilutions of antibodies were
394 prepared in media. SARS-CoV-2 pseudotyped VSV was diluted 1:30 in media in the presence
395 of 100 ng/mL anti-VSV-G antibody (clone 8G5F11, Absolute Antibody) and added 1:1 to each
396 antibody dilution. Virus:antibody mixtures were incubated for 1 hour at 37°C. Media was
397 removed from the cells and 50 µL of virus:antibody mixtures were added to the cells. One hour
398 post-infection, 100 µL of media was added to all wells and incubated for 17-20 hours at 37°C.
399 Media was removed and 50 µL of Bio-Glo reagent (Promega) was added to each well. The
400 plate was shaken on a plate shaker at 300 RPM at room temperature for 15 minutes and RLUs
401 were read on an EnSight plate reader (Perkin-Elmer).

402

403

404 *Transfection-based attachment receptor screen*

405 Lenti-X 293T cells (Takara) were transfected with plasmids encoding the following receptor
406 candidates (all purchased from Genecopoeia): ACE2 (NM_021804), DC-SIGN (NM_021155),
407 L-SIGN (BC110614), LGALS3 (NM_002306), SIGLEC1 (NM_023068), SIGLEC3
408 (XM_057602), SIGLEC9 (BC035365), SIGLEC10 (NM_033130), MGL (NM_182906),
409 MINCLE (NM_014358), CD147 (NM_198589), ASGR1 (NM_001671.4), ASGR2
410 (NM_080913), NRP1 (NM_003873). One day post transfection, cells were infected with
411 SARS-CoV-2 pseudotyped VSV at 1:20 dilution in the presence of 100 ng/mL anti-VSV-G
412 antibody (clone 8G5F11, Absolute Antibody) at 37°C. One hour post-infection, 100 µL of
413 media was added to all wells and incubated for 17-20 hours at 37°C. Media was removed and
414 50 µL of Bio-Glo reagent (Promega) was added to each well. The plate was shaken on a plate
415 shaker at 300 RPM at room temperature for 15 minutes and RLUs were read on an EnSight
416 plate reader (Perkin-Elmer).

417

418 *Trans-infection*

419 Parental HeLa cells or HeLa cells stably expressing DC-SIGN, L-SIGN or SIGLEC1 were
420 seeded at 5,000 cells per well in black-walled clear-bottom 96-well plates. One day later, cells
421 reached about 50% confluency and were inoculated with SARS-CoV-2 pseudotyped VSV at
422 1:10 dilution in the presence of 100 ng/mL anti-VSV-G antibody (clone 8G5F11, Absolute
423 Antibody) at 37°C for 2 h. For antibody-mediated inhibition of trans-infection, cells were pre-
424 incubated with 10 ug/mL anti-SIGLEC1 antibody (Biolegend, clone 7-239) for 30 min. After
425 2 h inoculation, cells were washed four times with complete medium and 10,000 VeroE6-
426 TMPRSS2 cells per well were added and incubated 17-20 h at 37°C for trans-infection. Media
427 was removed and 50 µL of Bio-Glo reagent (Promega) was added to each well. The plate was
428 shaken on a plate shaker at 300 RPM at room temperature for 15 minutes and RLUs were read
429 on an EnSight plate reader (Perkin-Elmer).

430

431 *Cell-cell fusion of CHO-S cells*

432 CHO cells stably expressing SARS-CoV-2 S-glycoprotein were seeded in 96 well plates for
433 microscopy (Thermo Fisher Scientific) at 12'500 cells/well and the following day, different
434 concentrations of mAbs and nuclei marker Hoechst (final dilution 1:1000) were added to the
435 cells and incubated for additional 24h hours. Fusion degree was established using the Cytation
436 5 Imager (BioTek) and an object detection protocol was used to detect nuclei as objects and
437 measure their size. The nuclei of fused cells (i.e., syncytia) are found aggregated at the center

438 of the syncytia and are recognized as a unique large object that is gated according to its size.
439 The area of the objects in fused cells divided by the total area of all the object multiplied by
440 100 provides the percentage of fused cells

441

442 *Negative stain EM imaging the fusogenic rearrangement of soluble S trimers*

443 SARS-CoV-2 S ectodomain trimer was engineered as follow and recombinantly expressed.
444 The D614G SARS-CoV-2 S has a mu-phosphatase signal peptide beginning at 14Q, a mutated
445 S1/S2 cleavage site (SGAR), ends at residue 1211K and followed by a TEV cleavage, fold-on
446 trimerization motif, and an 8X his tag in the pCMV vector. 10 μ M S was incubated with 13uM
447 Fab/protein for 1 or 48 hours at room temperature. Samples were diluted to be 0.01 mg/mL
448 immediately before protein was adsorbed to glow-discharged carbon-coated copper grids for
449 ~30seconds prior to a 2% uranyl formate staining. Micrographs were recorded using the
450 Leginon software⁴⁸ on a 100kV FEI Tecnai G2 Spirit with a Gatan Ultrascan 4000 4k x 4k
451 CCD camera at 67,000 nominal magnification. The defocus ranged from 1.0 to 2.0 μ m and the
452 pixel size was 1.6 Å.

453

454 *Cryo-electron microscopy*

455 SARS-CoV-2 HexaPro S⁴⁹ at 1.2 mg/mL was incubated with 1.2 fold molar excess of
456 recombinantly purified S2X58 for 10 seconds at room temperature before application onto a
457 freshly glow discharged 2.0/2.0 UltrAuFoil grid (200 mesh). Plunge freezing used a vitrobot
458 MarkIV (Thermo Fisher Scientific) using a blot force of 0 and 6.5 second blot time at 100%
459 humidity and 23°C.

460 Data were acquired using an FEI Titan Krios transmission electron microscope
461 operated at 300 kV and equipped with a Gatan K2 Summit direct detector and Gatan Quantum
462 GIF energy filter, operated in zero-loss mode with a slit width of 20 eV. Automated data
463 collection was carried out using Leginon⁴⁸ at a nominal magnification of 130,000x with a pixel
464 size of 0.525 Å and stage tilt angles up to 35°. The dose rate was adjusted to 8 counts/pixel/s,
465 and each movie was acquired in super-resolution mode fractionated in 50 frames of 200 ms.
466 4,126 micrographs were collected with a defocus range between -0.5 and -3.0 μ m. Movie frame
467 alignment, estimation of the microscope contrast-transfer function parameters, particle picking,
468 and extraction were carried out using Warp⁵⁰. Particle images were extracted with a box size
469 of 800 binned to 400 pixels² yielding a pixel size of 1.05 Å.

470 Two rounds of reference-free 2D classification were performed using CryoSPARC⁵¹ to
471 select well-defined particle images. These selected particles were subjected to two rounds of

472 3D classification with 50 iterations each (angular sampling 7.5° for 25 iterations and 1.8° with
473 local search for 25 iterations), using our previously reported closed SARS-CoV-2 S structure
474 as initial model (PDB 6VXX) in Relion⁵². 3D refinements were carried out using non-uniform
475 refinement along with per-particle defocus refinement in CryoSPARC⁵³. Selected particle
476 images were subjected to the Bayesian polishing procedure implemented in Relion3.0⁵⁴ before
477 performing another round of non-uniform refinement in CryoSPARC followed by per-particle
478 defocus refinement and again non-uniform refinement. Local resolution estimation, filtering,
479 and sharpening were carried out using CryoSPARC. Reported resolutions are based on the
480 gold-standard Fourier shell correlation (FSC) of 0.143 criterion and Fourier shell correlation
481 curves were corrected for the effects of soft masking by high-resolution noise substitution.
482 UCSF ChimeraX⁵⁵ and Coot⁵⁶ were used to fit atomic models into the cryoEM maps.

483

484 *Immunofluorescence analysis*

485 HEK293T-derived cell lines were seeded onto poly-D-Lysine-coated 96-well plates (Sigma-
486 Aldrich) and fixed 24 h after seeding with 4% paraformaldehyde for 30 min, followed by two
487 PBS (pH 7.4) washes and permeabilization with 0.25% Triton X-100 in PBS for 30 min. Cells
488 were incubated with primary antibodies anti-DC-SIGN/L-SIGN (Biolegend, cat. 845002,
489 1:500 dilution), anti-DC-SIGN (Cell Signaling, cat. 13193S, 1:500 dilution), anti-SIGLEC1
490 (Biolegend, cat. 346002, 1:500 dilution) or anti-ACE2 (R&D Systems, cat. AF933, 1:200
491 dilution) diluted in 3% milk powder/PBS for 2 h at room temperature. After washing and
492 incubation with a secondary Alexa647-labeled antibody mixed with 1 µg/ml Hoechst33342 for
493 1 hour, plates were imaged on an inverted fluorescence microscope (Echo Revolve).

494

495 *ACE2/TMPRSS2 RT-qPCR*

496 RNA was extracted from the cells using the NucleoSpin RNA Plus kit (Macherey-Nagel)
497 according to the manufacturer's protocol. RNA was reverse transcribed using the High
498 Capacity cDNA Reverse Transcription kit (Applied Biosystems) according to the
499 manufacturer's instructions. Intracellular levels of ACE2 (Forward Primer:
500 CAAGAGCAAACGGTTGAACAC, Reverse Primer: CCAGAGCCTCTCATTGTAGTCT),
501 HPRT (Forward Primer: CCTGGCGTCGTGATTAGTG, Reverse Primer:
502 ACACCCTTTCCAAATCCTCAG), and TMPRSS2 (Forward Primer:
503 CAAGTGCTCCRACTCTGGGAT, Reverse Primer: AACACACCGRTTCTCGTCCTC)
504 were quantified using the Luna Universal qPCR Master Mix (New England Biolabs) according
505 to the manufacturer's protocol. Levels of ACE2 and TMPRSS2 were normalized to HPRT.

506 HeLa cells were used as the reference sample. All qPCRs were run on a QuantStudio 3 Real-
507 Time PCR System (Applied Biosystems).

508

509 *SARS2 D614G Spike Production and biotinylation*

510 Prefusion-stabilized SARS2 D614G spike (comprising amino acid sequence Q14 to K1211)
511 with a C-terminal TEV cleavage site, T4 bacteriophage fibritin foldon, 8x His-, Avi- and
512 EPEA-tag was transfected into HEK293 Freestyle cells, using 293fectin as a transfection
513 reagent. Cells were left to produce protein for three days at 37°C. Afterwards, supernatant was
514 harvested by centrifuging cells for 30 minutes at 500 xg, followed by another spin for 30
515 minutes at 4000 xg. Cell culture supernatant was filtered through a 0.2 um filter and loaded
516 onto a 5 mL C-tag affinity matrix column, pre-equilibrated with 50 mM Tris pH 8 and 200 mM
517 NaCl. SARS2 D614G spike was eluted, using 10 column volumes of 100 mM Tris, 200 mM
518 NaCl and 3.8 mM SEPEA peptide. Elution peak was concentrated and injected on a Superose
519 6 increase 10/300 GL gel filtration column, using 50 mM Tris pH 8 and 200 mM NaCl as a
520 running buffer. SEC fractions corresponding to monodisperse SARS2 D614G spike were
521 collected and flash frozen in liquid nitrogen for storage at -80°C. Purified SARS2 D614G spike
522 protein was biotinylated using BirA500 biotinylation kit from Avidity. To 50 ug of spike
523 protein, 5 ug of BirA, and 11 uL of BiomixA and BiomixB was added. Final spike protein
524 concentration during the biotinylation reaction was ~1 uM. The reaction was left to proceed
525 for 16 hours at 4°C. Then, protein was desalted using two Zeba spin columns pre-equilibrated
526 with 1x PBS pH 7.4.

527

528 *Flow cytometry analysis for DC-SIGN, L-SIGN, SIGLEC1 and ACE-2*

529 HEK293T cells expressing DC-SIGN, L-SIGN, SIGLEC1 or ACE2 were resuspended at 4×10^6
530 cells/mL and 100 µL per well were seeded onto V-bottom 96-well plates (Corning, 3894). The
531 plate was centrifuged at 2,000 rpm for 5 minutes and washed with PBS (pH 7.4). The cells
532 were resuspended in 200 µL of PBS containing Ghost violet 510 viability dye (Cell Signaling,
533 cat. 13-0870-T100, 1:1,000 dilution), incubated for 15 minutes on ice and then washed. The
534 cells were resuspended in 100 µL of FACS buffer prepared with 0.5% BSA (Sigma-Aldrich)
535 in PBS containing the primary antibodies at a 1:100 dilution: mouse anti-DC/L-SIGN
536 (Biolegend, cat. 845002), rabbit anti-DC-SIGN (Cell Signaling, cat. 13193), mouse anti-
537 SIGLEC1 (Biolegend, cat. 346002) or goat anti-ACE2 (R&D Systems, cat. AF933). After 1 h
538 incubation on ice, the cells were washed two times and resuspended in FACS buffer containing
539 the Alexa Fluor-488-labeled secondary antibodies at a 1:200 dilution: goat anti-mouse

540 (Invitrogen cat. A11001), goat anti-rabbit (Invitrogen cat. A11008) or donkey anti-goat
541 (Invitrogen cat. A11055). After incubation for 45 min on ice, the cells were washed three times
542 with 200µL of FACS buffer and fixed with 200µL of 4% PFA (Alfa Aesar) for 15 mins at room
543 temperature. Cells were washed three times, resuspended in 200µL of FACS buffer and
544 analyzed by flow cytometry using the CytoFLEX flow cytometer (Beckman Coulter).

545

546 *Flow cytometry of SARS-CoV-2 Spike and RBD binding to cells*

547 Biotinylated SARS-CoV-2 Spike D614G protein (Spikebiotin, in-house generated) or the
548 biotinylated SARS-CoV-2 Spike receptor-binding domain (RBDbiotin, Sino Biological,
549 40592-V08B) were incubated with Alexa Fluor® 647 streptavidin (AF647-strep, Invitrogen,
550 S21374) at a 1:20 ratio by volume for 20 min at room temperature. The labeled proteins were
551 then stored at 4°C until further use. Cells were dissociated with TrpLE Express (Gibco, 12605-
552 010) and 10⁵ cells were transferred to each well of a 96-well V bottom plate (Corning, 3894).
553 Cells were washed twice in flow cytometry buffer (2% FBS in PBS (w/o Ca/Mg)) and stained
554 with Spikebiotin-AF647-strep at a final concentration of 20 µg/ml or RBDbiotin-AF647-strep
555 at a final concentration of 7.5 µg/ml for 1h on ice. Stained cells were washed twice with flow
556 cytometry buffer, resuspended in 1% PFA (Electron Microscopy Sciences, 15714-S) and
557 analyzed with the Cytotflex LX (Beckman Coulter).

558

559 *Recombinant expression of SARS-CoV-2-specific mAbs.*

560 Human mAbs were isolated from plasma cells or memory B cells of SARS-CoV-2 immune
561 donors, as previously described^{27,57,58}. Recombinant antibodies were expressed in ExpiCHO
562 cells at 37°C and 8% CO₂. Cells were transfected using ExpiFectamine. Transfected cells were
563 supplemented 1 day after transfection with ExpiCHO Feed and ExpiFectamine CHO Enhancer.
564 Cell culture supernatant was collected eight days after transfection and filtered through a 0.2
565 µm filter. Recombinant antibodies were affinity purified on an ÄKTA xpress FPLC device
566 using 5 mL HiTrap™ MabSelect™ Prisma columns followed by buffer exchange to Histidine
567 buffer (20 mM Histidine, 8% sucrose, pH 6) using HiPrep 26/10 desalting columns

568

569 *SARS-CoV-2 infection model in hamster*

570 *Virus preparation.* The SARS-CoV-2 strain used in this study, BetaCov/Belgium/GHB-
571 03021/2020 (EPI_ISL_109_407976|2020-02-03), was recovered from a nasopharyngeal swab
572 taken from an RT-qPCR confirmed asymptomatic patient who returned from Wuhan, China in
573 February 2020. A close relation with the prototypic Wuhan-Hu-1 2019-nCoV (GenBank

574 accession 112 number MN908947.3) strain was confirmed by phylogenetic analysis. Infectious
575 virus was isolated by serial passaging on HuH7 and Vero E6 cells⁵⁹; passage 6 virus was used
576 for the study described here. The titer of the virus stock was determined by end-point dilution
577 on Vero E6 cells by the Reed and Muench method⁶⁰. Live virus-related work was conducted
578 in the high-containment ABSL3 and BSL3+ facilities of the KU Leuven Rega Institute
579 (3CAPS) under licenses AMV 30112018 SBB 219 2018 0892 and AMV 23102017 SBB 219
580 20170589 according to institutional guidelines.

581 *Cells.* Vero E6 cells (African green monkey kidney, ATCC CRL-1586) were cultured in
582 minimal essential medium (Gibco) supplemented with 10% fetal bovine serum (Integro), 1%
583 L- glutamine (Gibco) and 1% bicarbonate (Gibco). End-point titrations were performed with
584 medium containing 2% fetal bovine serum instead of 10%.

585 *SARS-CoV-2 infection model in hamsters.* The hamster infection model of SARS-CoV-2 has
586 been described before^{59,61}. The specific study design is shown in the schematic below. In brief,
587 wild-type Syrian Golden hamsters (*Mesocricetus auratus*) were purchased from Janvier
588 Laboratories and were housed per two in ventilated isolator cages (IsoCage N Biocontainment
589 System, Tecniplast) with *ad libitum* access to food and water and cage enrichment (wood
590 block). The animals were acclimated for 4 days prior to study start. Housing conditions and
591 experimental procedures were approved by the ethics committee of animal experimentation of
592 KU Leuven (license P065- 2020). Female 6-8 week old hamsters were anesthetized with
593 ketamine/xylazine/atropine and inoculated intranasally with 50 μ L containing 2×10^6 TCID₅₀
594 SARS-CoV-2 (day 0).

595 *Treatment regimen.* Animals were prophylactically treated 48h before infection by
596 intraperitoneal administration (i.p.) and monitored for appearance, behavior, and weight. At
597 day 4 post infection (p.i.), hamsters were euthanized by i.p. injection of 500 μ L Dolethal (200
598 mg/mL sodium pentobarbital, Vétoquinol SA). Lungs were collected and viral RNA and
599 infectious virus were quantified by RT-qPCR and end-point virus titration, respectively. Blood
600 samples were collected before infection for PK analysis.

601 *SARS-CoV-2 RT-qPCR.* Collected lung tissues were homogenized using bead disruption
602 (Precellys) in 350 μ L RLT buffer (RNeasyMinikit, Qiagen) and centrifuged (10.000 rpm, 5 min)
603 to pellet the cell debris. RNA was extracted according to the manufacturer's instructions. Of
604 50 μ L eluate, 4 μ L was used as a template in RT-qPCR reactions. RT-qPCR was performed on
605 a LightCycler96 platform (Roche) using the iTaq Universal Probes One-Step RT-qPCR kit
606 (BioRad) with N2 primers and probes targeting the nucleocapsid⁵⁹. Standards of SARS-CoV-
607 2 cDNA (IDT) were used to express viral genome copies per mg tissue or per mL serum.

608 *End-point virus titrations.* Lung tissues were homogenized using bead disruption (Precellys)
609 in 350 μ L minimal essential medium and centrifuged (10,000 rpm, 5min, 4°C) to pellet the cell
610 debris. To quantify infectious SARS-CoV-2 particles, endpoint titrations were performed on
611 confluent Vero E6 cells in 96- well plates. Viral titers were calculated by the Reed and Muench
612 method⁶⁰ using the Lindenbach calculator and were expressed as 50% tissue culture infectious
613 dose (TCID₅₀) per mg tissue.

614 *Histology.* For histological examination, the lungs were fixed overnight in 4% formaldehyde
615 and embedded in paraffin. Tissue sections (5 μ m) were analyzed after staining with
616 hematoxylin and eosin and scored blindly for lung damage by an expert pathologist. The scored
617 parameters, to which a cumulative score of 1 to 3 was attributed, were the following:
618 congestion, intra-alveolar hemorrhagic, apoptotic bodies in bronchus wall, necrotizing
619 bronchiolitis, perivascular edema, bronchopneumonia, perivascular inflammation,
620 peribronchial inflammation and vasculitis.

621 *Binding of immunocomplexes to hamster monocytes.* Immunocomplexes (IC) were generated
622 by complexing S309 mAb (hamster IgG, either wt or N297A) with a biotinylated anti-idiotypic
623 Fab fragment and Alexa-488-streptavidin, using a precise molar ratio (4:8:1, respectively). Pre-
624 generated fluorescent IC were serially diluted incubated at 4°C for 3 hrs with freshly revitalized
625 hamster splenocytes, obtained from a naïve animal. Cellular binding was then evaluated by
626 cytometry upon exclusion of dead cells and physical gating on monocyte population. Results
627 are expressed as Alexa-488 mean fluorescent intensity of the entire monocyte population.

628

629 *Bioinformatic analyses*

630 Processed Human Lung Cell Atlas (HLCA) data and cell-type annotations were downloaded
631 from Github (<https://github.com/krasnowlab/HLCA>)²¹. Processed single-cell transcriptome
632 data and annotation of lung epithelial and immune cells from SARS-CoV-2 infected
633 individuals were downloaded from NCBI GEO database (ID: GSE158055)²² and Github
634 (https://github.com/zhangzlab/covid_balf)²³. Available sequence data from the second single-
635 cell transcriptomics study by Liao et al²³ were downloaded from NCBI SRA (ID:
636 PRJNA608742) for inspection of reads corresponding to viral RNA. The proportion of sgRNA
637 relative to genomic RNA was estimated by counting TRS-containing reads supporting a leader-
638 TRS junction. Criteria and methods for detection of leader-TRS junction reads were adapted
639 from Alexandersen et al.⁶². The viral genome reference and TRS annotation was based on
640 Wuhan-Hu-1 NC_045512.2/MN908947⁶³. Only 2 samples from individuals with severe
641 COVID-19 had detectable leader-TRS junction reads (SRR11181958, SRR11181959).

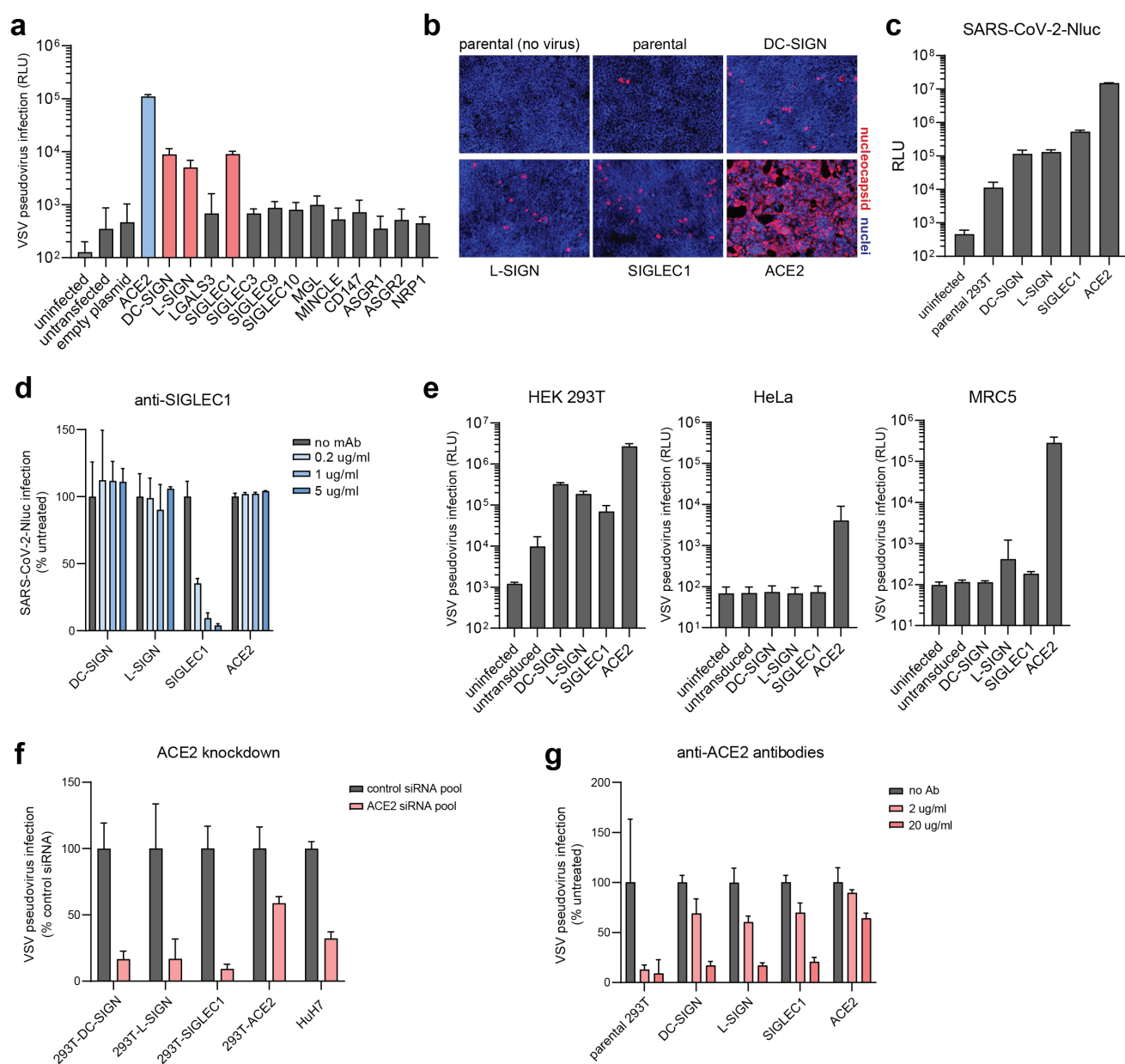


Fig. 1. DC-SIGN, L-SIGN and SIGLEC1 function as auxiliary receptors for SARS-CoV-2 infection. **a**, VSV-SARS-CoV-2 pseudovirus infection of HEK293T cells transfected to over-express ACE2 or a panel of selected lectins and published receptor candidates. **b**, Stable HEK293T cell lines overexpressing DC-SIGN, L-SIGN, SIGLEC1 or ACE2 were infected with authentic SARS-CoV-2 (MOI 0.1), fixed and immunostained at 24 hours for the SARS-CoV-2 nucleocapsid protein (red). **c**, HEK293T stable cell lines were infected with SARS-CoV-2-Nluc and luciferase levels were quantified at 24 hours. **d**, Stable cell lines were incubated with different concentrations of anti-SIGLEC1 mAb (clone 7-239) and infected with SARS-CoV-2-Nluc. **e**, HEK293T, HeLa and MRC5 cells were transiently transduced to overexpress DC-SIGN, L-SIGN, SIGLEC1 or ACE2 and infected with VSV-SARS-CoV-2 pseudovirus. **f**, Stable cell lines were treated with ACE2 siRNA followed by infection with VSV-SARS-CoV-2 pseudovirus four days post transfection. **g**, Stable cell lines were incubated with different concentrations of anti-ACE2 goat polyclonal antibodies and infected with VSV-SARS-CoV-2 pseudovirus.

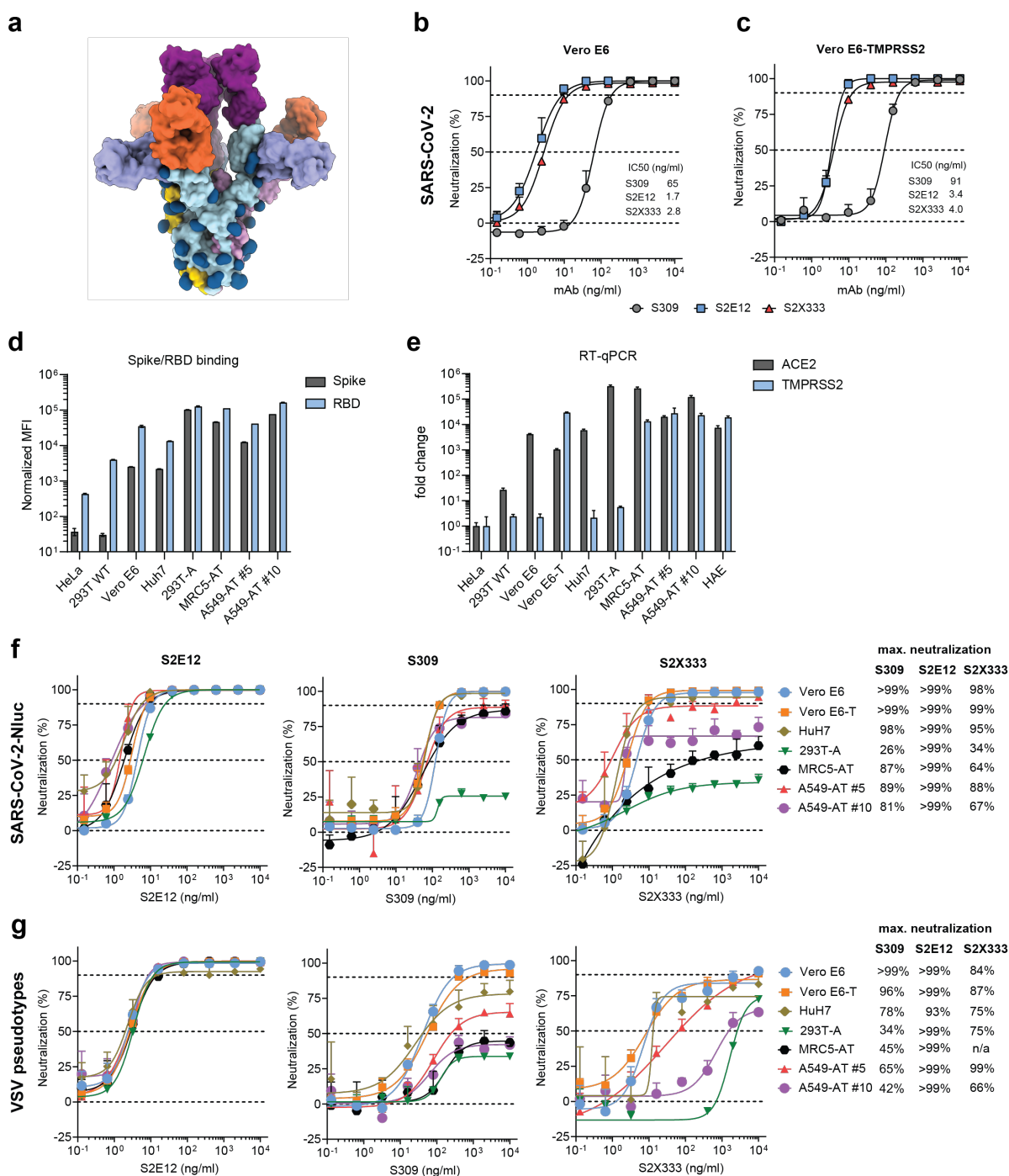


Fig. 3. ACE2 over-expression influences neutralizing activity by different classes of anti-spike mAbs. **a**, Surface rendering of a composite model of SARS-CoV-2 S bound to S309 (purple), S2E12 (magenta) and S2X333 (orange)^{5, 27, 28}. The three SARS-CoV-2 S protomers are colored light blue, gold and pink whereas N-linked glycans are rendered dark blue. **b-c**, SARS-CoV-2 neutralization with S309, S2E12 and S2X333 on (b) Vero E6 or (c) Vero E6-TMPRSS2 cells. Cells were infected with SARS-CoV-2 (isolate USA-WA1/2020) at MOI 0.01 in the presence of the respective mAbs. Cells were fixed 24h post infection, viral nucleocapsid protein was immunostained and quantified. **d**, Purified, fluorescently-labeled SARS-CoV-2 spike or RBD protein binding to the indicated cell lines was quantified by flow cytometry. “A”: ACE2, “T”: TMPRSS2 **e**, Cellular ACE2 and TMPRSS2 transcripts were quantified by RT-qPCR. **f-g**, A panel of 7 cell lines were infected with SARS-CoV-2-Nluc **f**, or VSV-SARS-CoV-2 pseudovirus (**g**) in the presence of S309, S2E12 or S2X333. Luciferase signal was quantified 24h post infection.

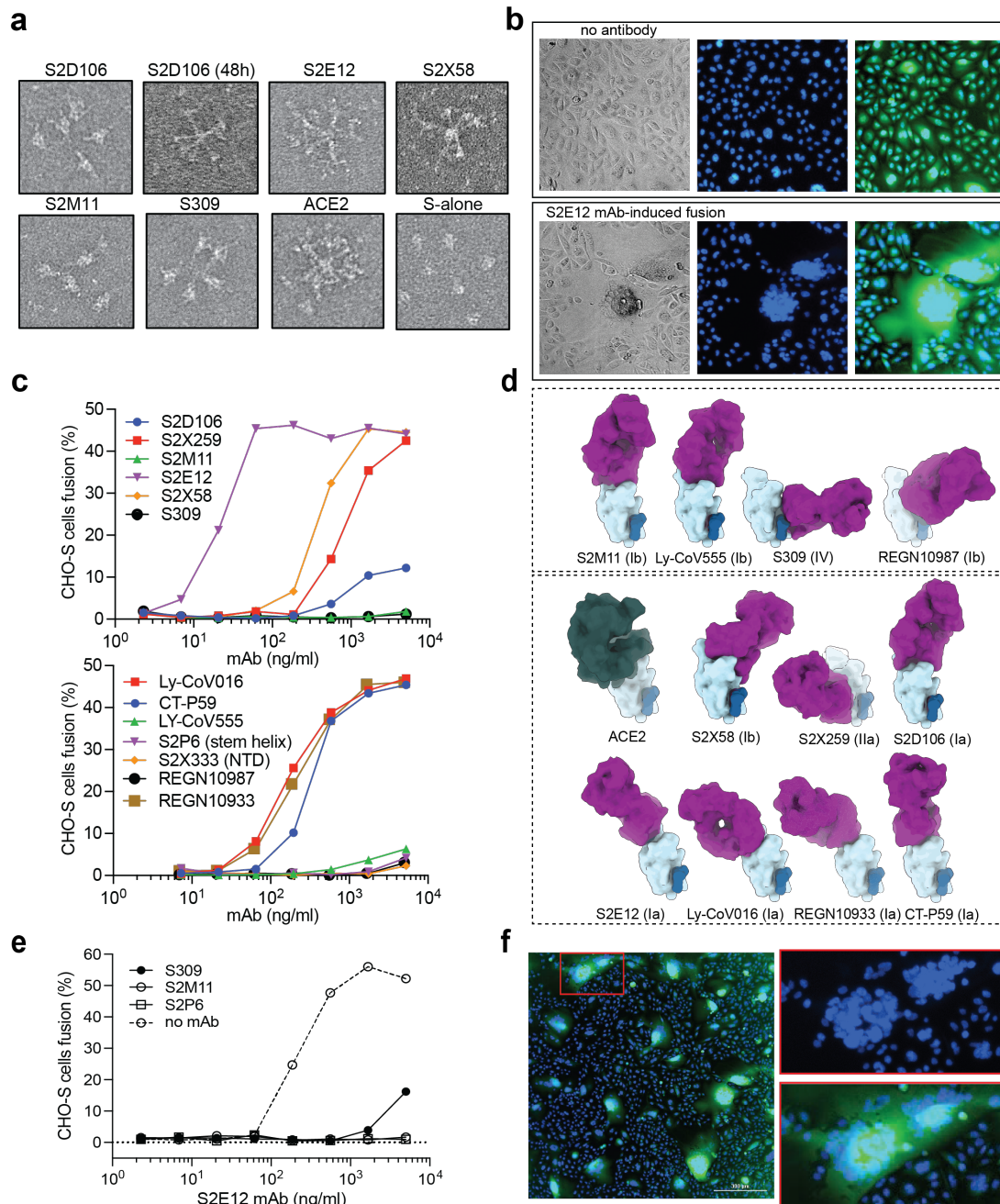


Fig. 4. RBM mAbs trigger the fusogenic rearrangement of the S protein and promote membrane fusion. **a**, MAbs or soluble ACE2 were incubated for 1 hour with native-like soluble prefusion S trimer of SARS-CoV-2 to track by negative stain EM imaging the fusogenic rearrangement of soluble S trimers visible as rosettes. **b**, Cell-cell fusion of CHO cells expressing SARS-CoV-2 S (CHO-S) on the plasma membrane in the absence (upper panel) or presence of 5 $\mu\text{g/ml}$ of S2E12 mAb (lower panel) as detected by immunofluorescence. Nuclei stained with Hoechst dye; cytoplasm stained with CellTracker Green. **(c)**, CHO-S cell-cell fusion mediated by different spike-specific mAbs quantified as described in Methods. **d**, Structures of 11 Fab-RBD complexes related to mAbs used in (c) (RBD orientation is fixed) and of ACE2-RBD as determined by a combination of X-ray crystallography and cryo-EM analysis (PDBs, **Extended Data Table 1**). Shown in parentheses the RBD antigenic site as defined according to Piccoli et al.³ **e**, Inhibition of S2E12-induced cell-cell fusion performed as in (c) by a fixed amount (15 $\mu\text{g/ml}$) of indicated mAbs. **f**, Trans-fusion of S-positive CHO cells with S-negative fluorescently-labelled CHO cells. Staining as in (b).

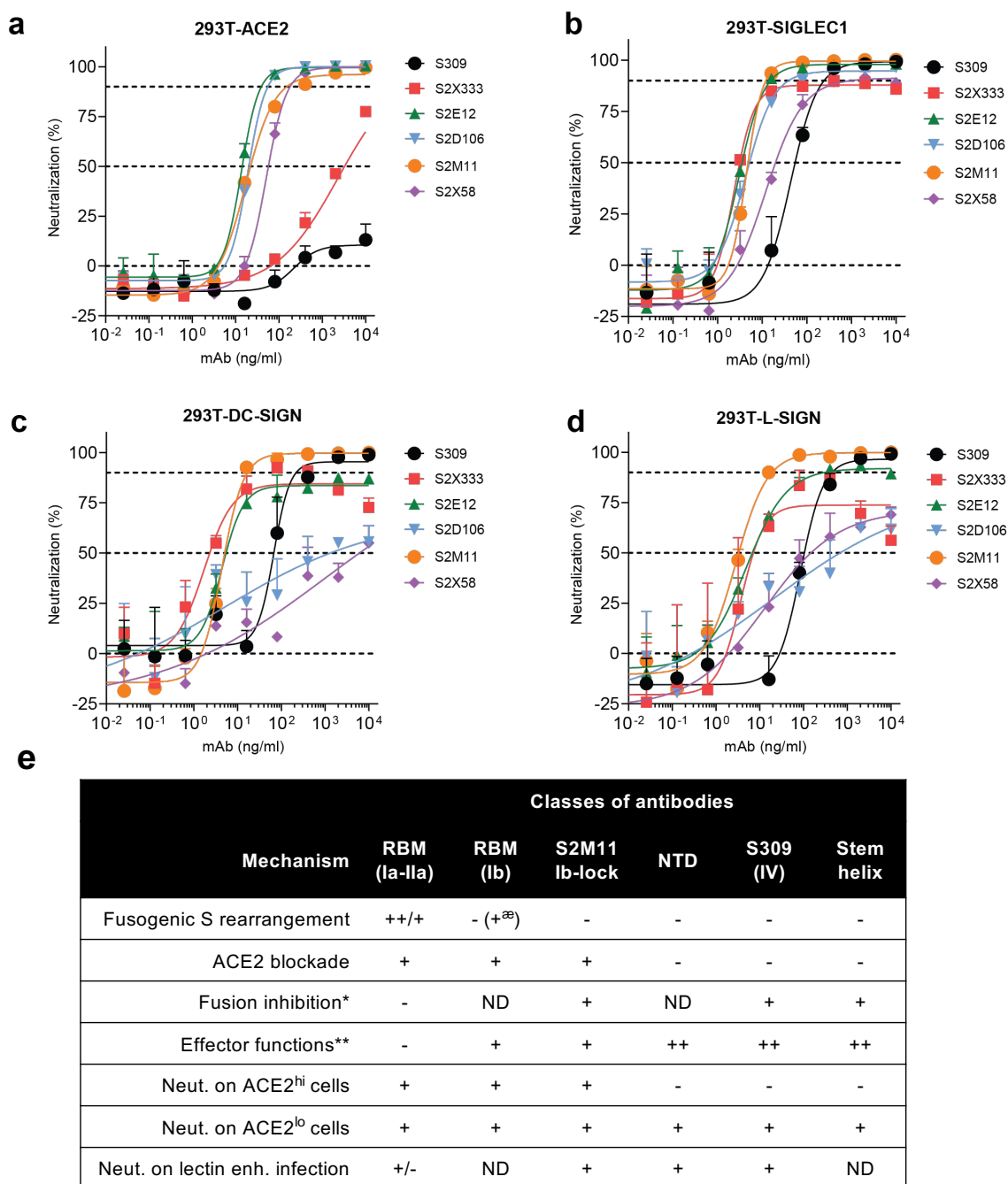
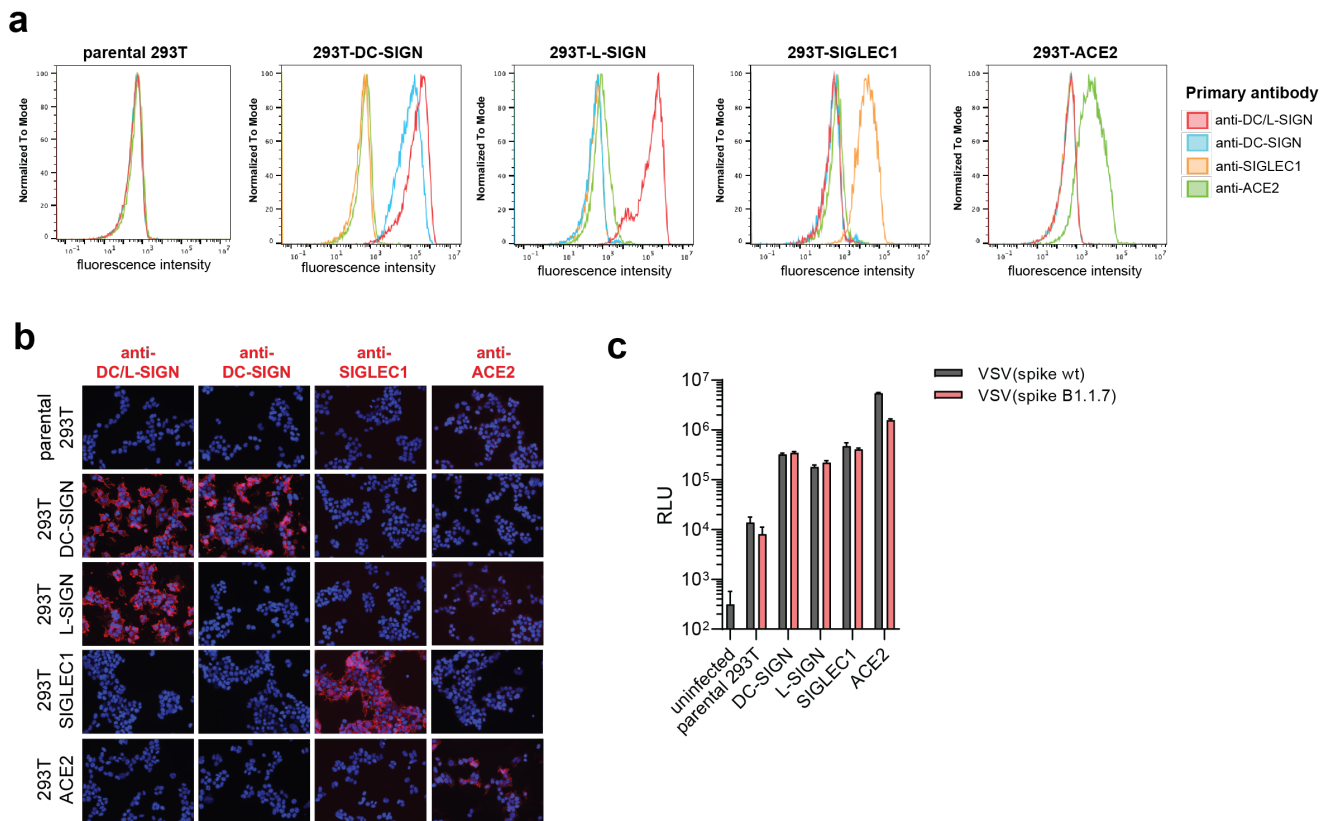
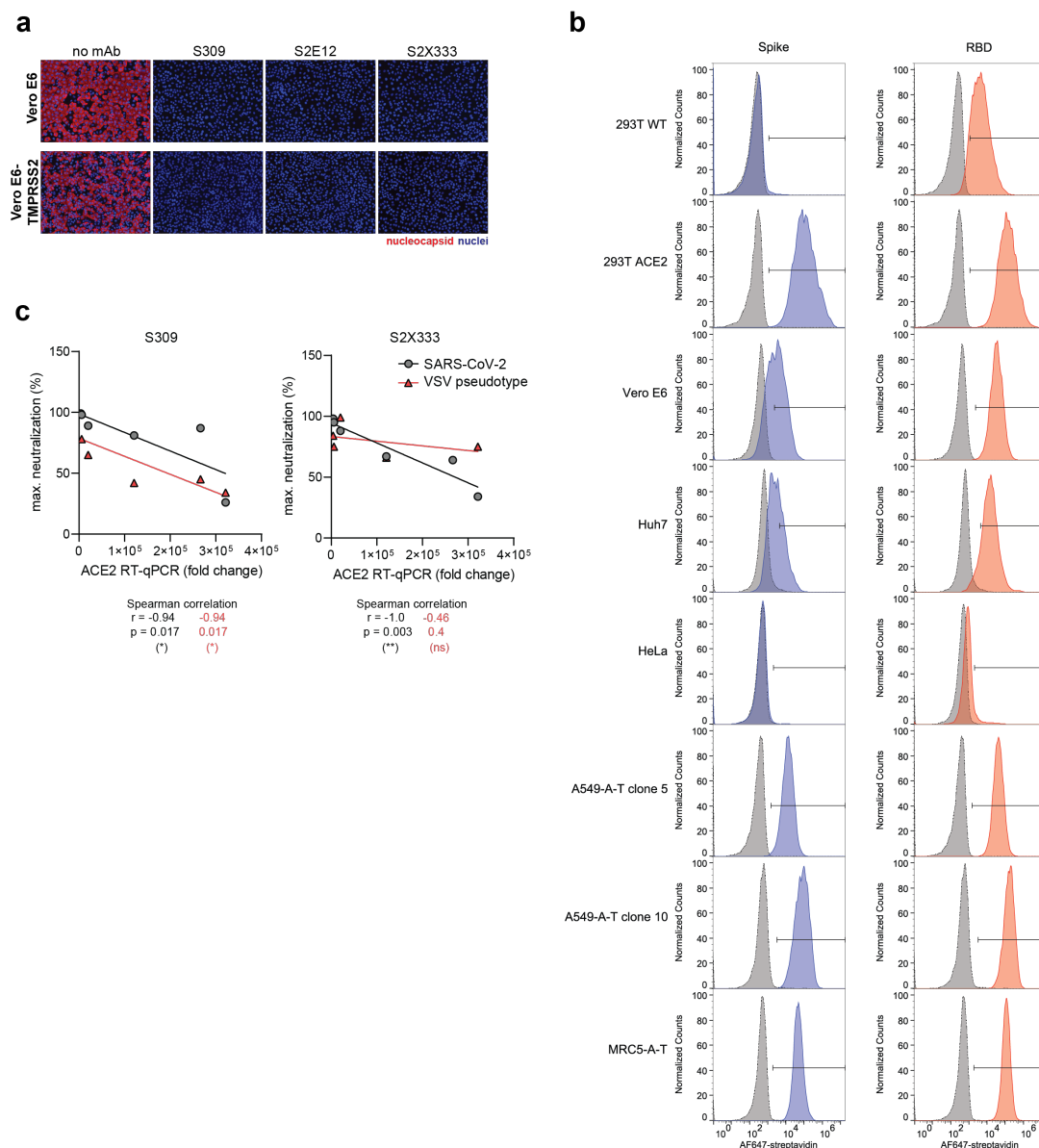


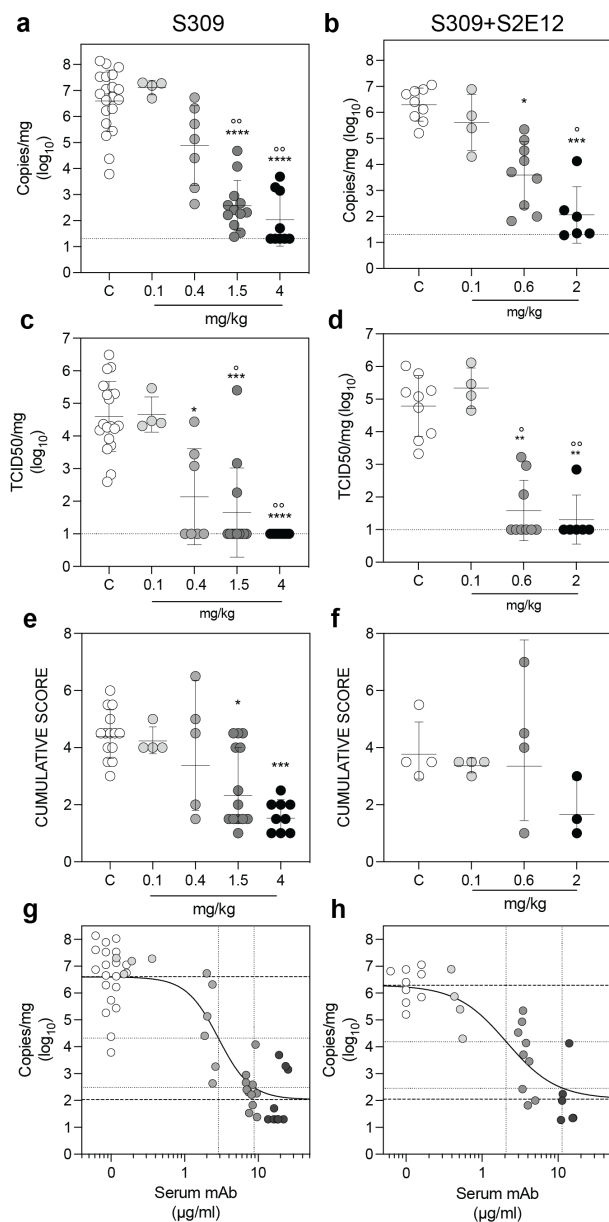
Fig. 5. SIGLEC1, DC-SIGN and L-SIGN modulate neutralizing activity by different classes of antibodies. a-d, Neutralization of infection by authentic SARS-CoV-2 pre-incubated with indicated mAbs of HEK293T cell lines stably overexpressing DC-SIGN, L-SIGN, SIGLEC1 or ACE2. Infection was measured by immunostaining at 24 hours for the SARS-CoV-2 nucleoprotein. e, Summary of the mechanisms of action of different classes of spike-specific mAbs based on this and previous studies. *, mAb-mediated inhibition of fusion between CHO-spike cells and ACE2⁺ Vero-E6 cells; **, based on mAb-dependent activation of human FcγRs performed with a bioluminescent reporter assay as in²⁷. ^æ, S2X58 binds to open RBM due to a conformational clash with neighboring NTD



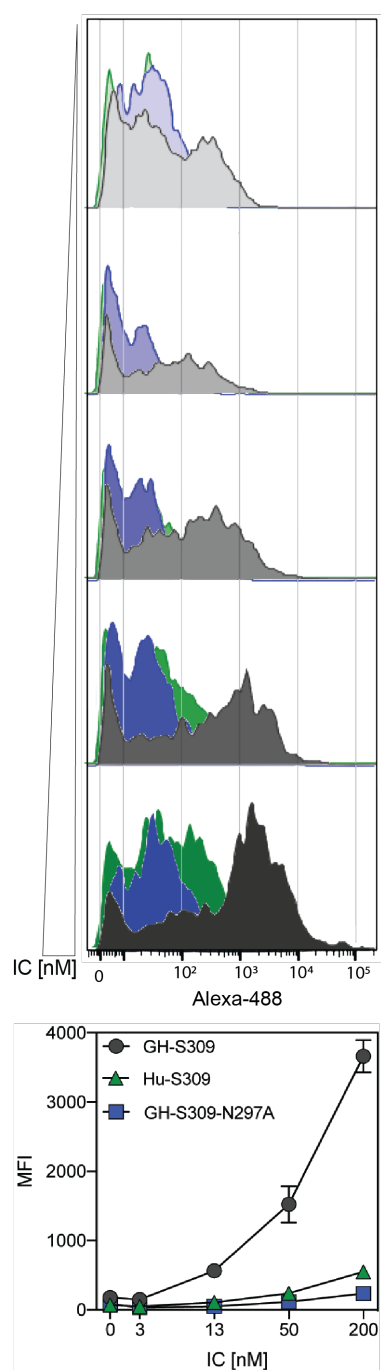
Extended Data Fig. 1. Characterization of DC-SIGN, L-SIGN and SIGLEC-1 as SARS-CoV-2 attachment factors. a-b, Binding of antibodies targeting DC-/L-SIGN, DC-SIGN, SIGLEC1 or ACE2 on HEK293T stably over-expressing the respective attachment receptors was analyzed by flow cytometry (a) and immunofluorescence analysis (b). **c,** HEK293T cells over-expressing the respective attachment receptors were infected with VSV-SARS-COV-2 wildtype spike (grey bars) or spike bearing mutations of the B.1.1.7 variant (red bars). Luminescence was analyzed one day post infection.



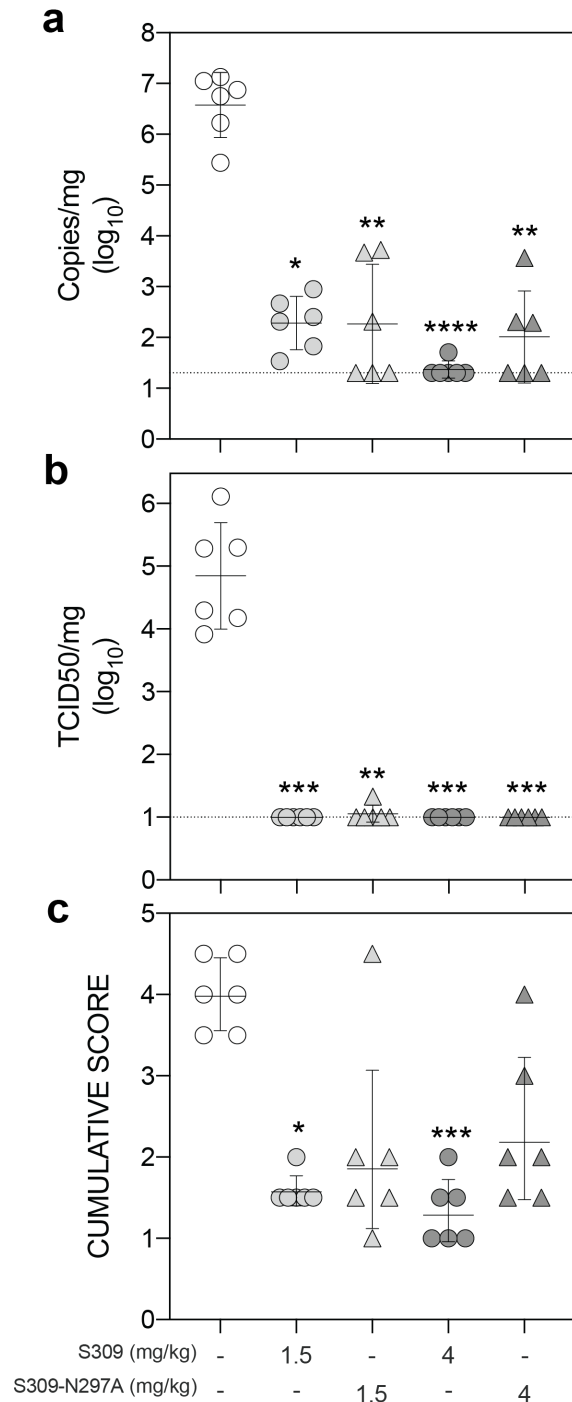
Extended Data Fig. 2: Characterization of SARS-CoV-2-susceptible cell lines. **a**, SARS-CoV-2 neutralization with 10 μ g/ml of S309, S2E12 and S2X333 on Vero E6 or Vero E6-TMPRSS2 cells. Cells were infected with SARS-CoV-2 (isolate USA-WA1/2020) at MOI 0.01 in the presence of the respective mAbs. Cells were fixed 24h post infection and viral nucleocapsid protein was immunostained. **b**, Purified, fluorescently-labelled SARS-CoV-2 spike protein or RBD protein was incubated with the indicated cell lines and protein binding was quantified by flow cytometry. **c**, Correlation analysis between ACE2 transcript levels and maximum antibody neutralization in all SARS-CoV-2-susceptible cell lines.



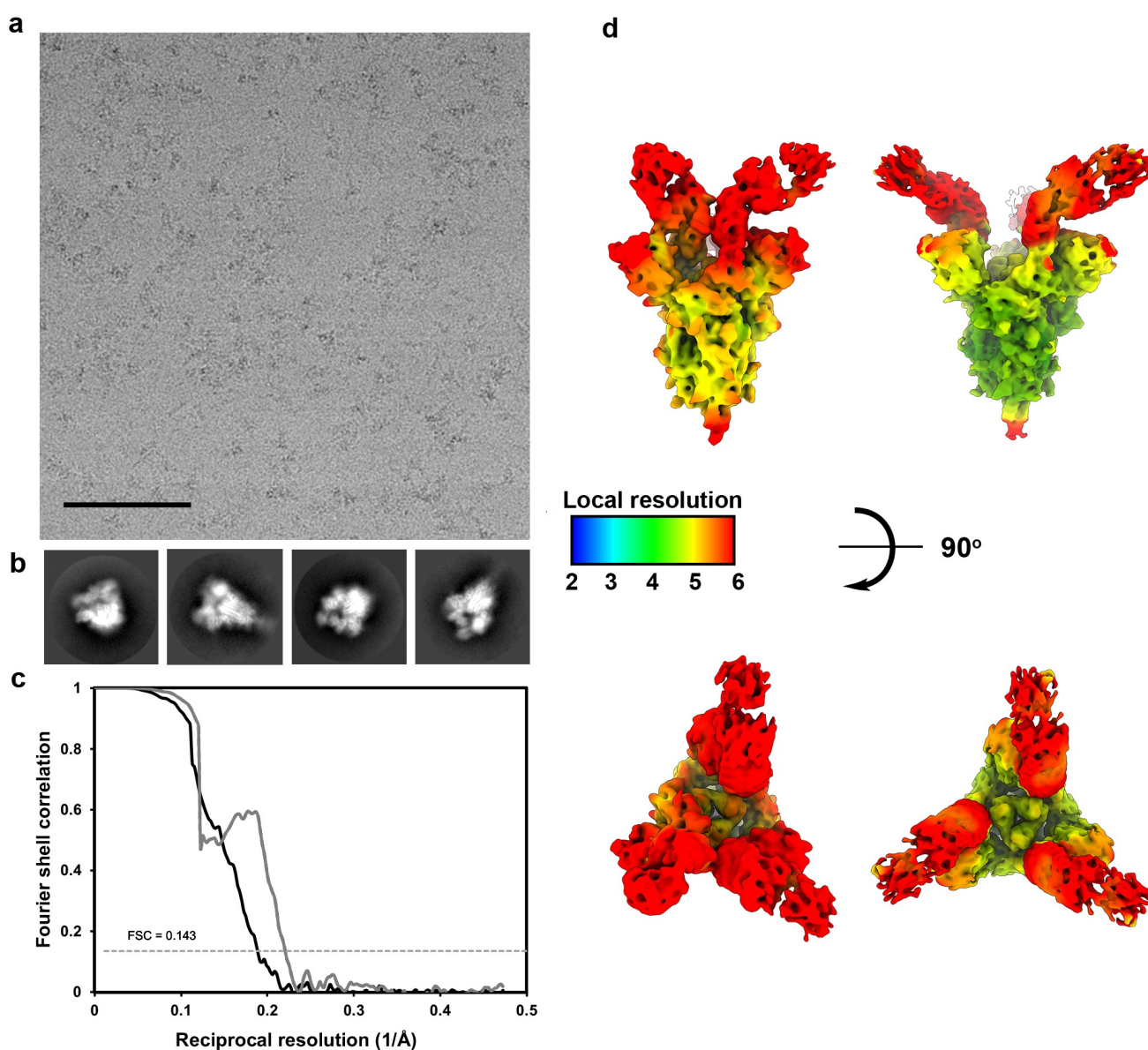
Extended Data Fig. 3: S309 or a cocktail of S309 and S2E12 provide robust in vivo protection against SARS-CoV-2 challenge. Syrian hamsters were injected with the indicated amount of mAb(s) 48 hours before intra-nasal challenge with SARS-CoV-2. **(a-b)** Quantification of viral RNA in the lungs 4 days post-infection. **(c-d)** Quantification of replicating virus in lung homogenates harvested 4 days post infection using a TCID50 assay. **(e-f)** Histopathological score of the lung tissue was assessed 4 days post infection. **(g-h)** Efficacy plots based on the correlation between the level of serum antibody measured at the time of infection and the level of SARS-CoV2 (viral RNA) measured in lungs on day 4 after infection. The dotted lines represents EC50 and EC90 for viral reduction (EC90 of S309 alone vs S309+S2E12: 9 vs 11 $\mu\text{g/ml}$, respectively).



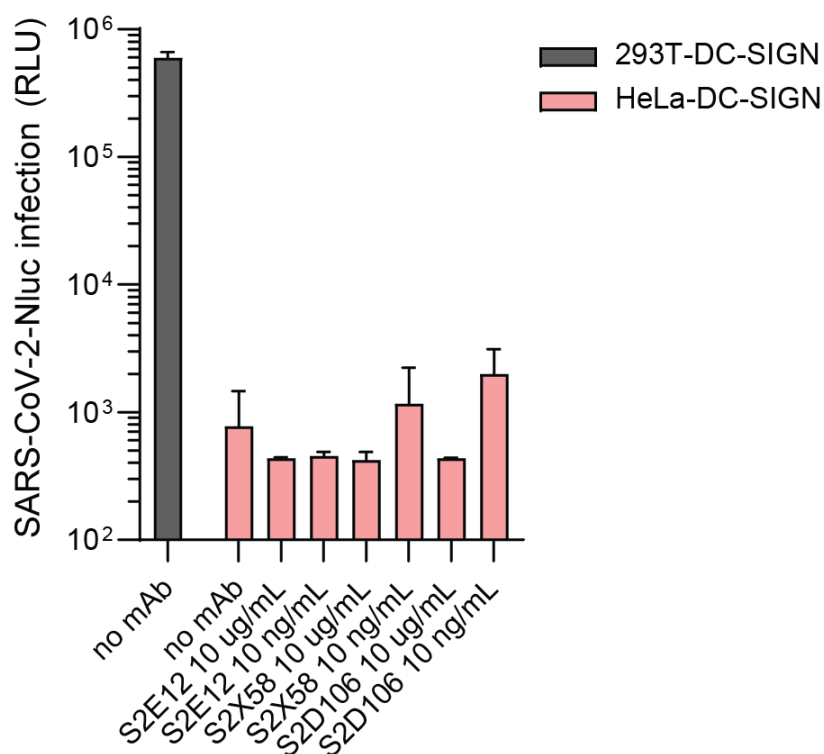
Extended Data Fig. 4: Binding of immunocomplexes to hamster splenocytes. Alexa-488 fluorescent IC were titrated (0-200 nM range) and incubated with total naïve hamster splenocytes. Binding was revealed with a cytometer upon exclusion of dead/apoptotic cells and physical gating on bona fide monocyte population. Top panel shows the fluorescent intensity associated to hamster cells of IC made with either hamster Fc antibodies (human S309, green, GH-S309, dark grey and GH-S309-N297A, blue). A single replicate of two is shown. Bottom Panel show the relative Alexa-488 mean fluorescent intensity of the replicates measured on the entire monocyte population.



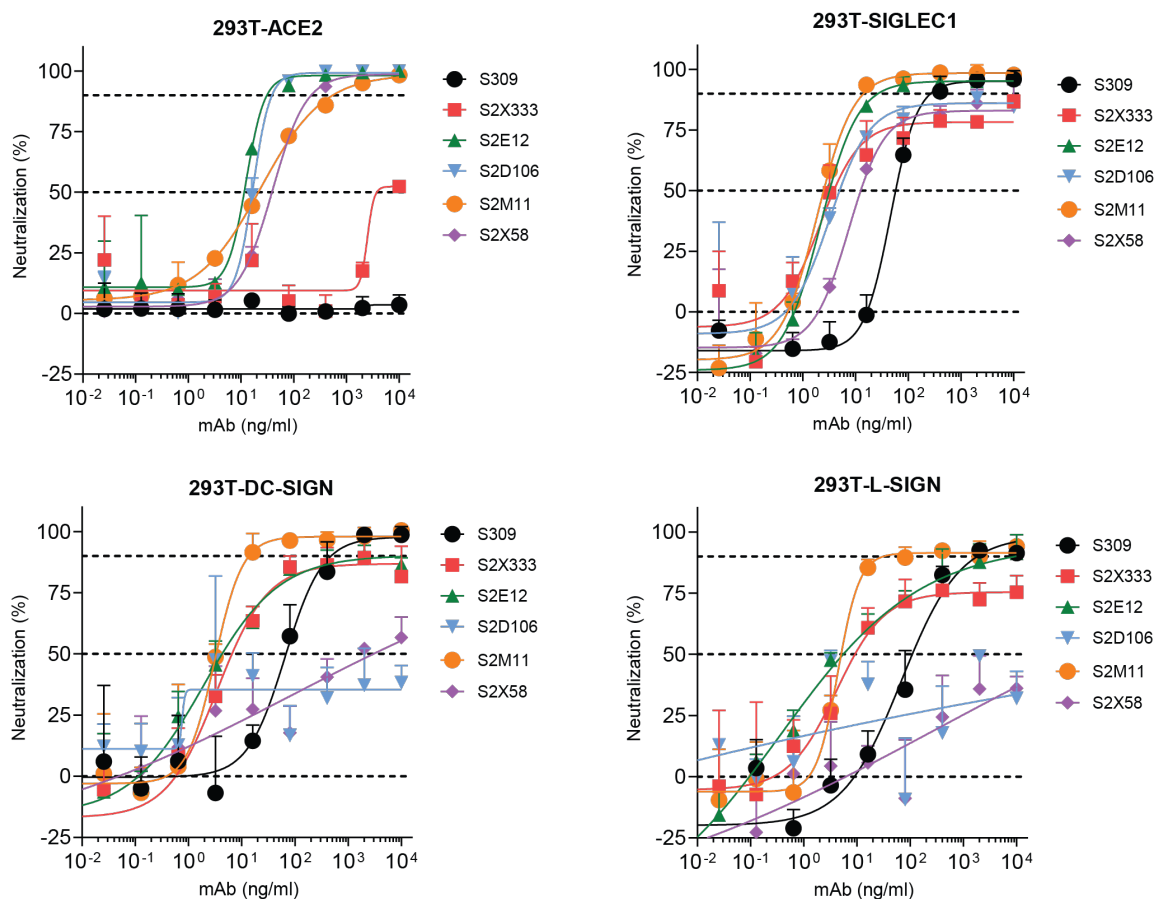
Extended Data Fig. 5: Role of host effector function in SARS-CoV-2 challenge. Syrian hamsters were injected with the indicated amount (mg/kg) of hamster IgG2a S309 either wt or Fc silenced (S309-N297A). **a**, Quantification of viral RNA in the lung 4 days post infection. **b**, Quantification of replicating virus in the lung 4 days post infection. **c**, Histopathological score in the lung 4 days post infection. Control animals (white symbols) were injected with 4 mg/kg unrelated control isotype mAb. *, **, ***, **** p< 0.05, 0.01, 0.001, 0.0001 respectively vs control animals. Mann-Whitney test.



Extended Data Fig. 6: Data collection and processing of the S/S2X58 complex cryoEM datasets. **a,b**, Representative electron micrograph and 2D class averages of SARS-CoV-2 S in complex with the S2X58 Fab embedded in vitreous ice. Scale bar: 400 Å. **c**, Gold-standard Fourier shell correlation curves for the S2X58-bound SARS-CoV-2 S trimer in one RBD closed (black line) and three RBDs open conformations (gray line). The 0.143 cutoff is indicated by a horizontal dashed line. **d**, Local resolution maps calculated using cryoSPARC for the SARS-CoV-2 S/S2X58 Fab complex structure with one RBD closed and three RBDs open shown in two orthogonal orientations.



Extended Data Fig. 7: HeLa cells expressing DC-SIGN are refractory to SARS-CoV-2 infection. 293T or HeLa cells stably expressing DC-SIGN were infected with SARS-CoV-2-Nluc at MOI0.04 in the presence of the indicated antibodies. Infection was analyzed by quantification of luminescent signal at 24 h post infection.



Extended Data Fig. 8: SARS-CoV-2 live virus neutralization. HEK293T cells stably expressing ACE2, SIGLEC1, DC-SIGN or L-SIGN were infected with SARS-CoV-2 at MOI 0.02 in the presence of the indicated mAbs. Cells were fixed 24h post infection, viral nucleocapsid protein was immunostained and positive cells were quantified.

Extended Data Table 1. MABs used in this study.

MAB	Alias or derived mAb(s)	Domain (site)	ACE2 blocking	SARS-CoV	Phase	PDB	Ref
S309	VIR-7831/VIR-7832	RBD (IV)	-	+	EUA submitted	7IX3	27
S2E12		RBD (Ia)	+	-	preclinical	7K4N	5
S2M11		RBD (Ib-lock)	+	-	preclinical	7K43	5
S2P6		S2 (stem helix)	-	+	preclinical	xxx	manuscript in preparation
S2X58		RBD (Ib)	+	-	preclinical	this study	Starr et al. submitted
S2D106		RBD (Ia)	+	-	preclinical	xxx	Starr et al. submitted
S2X259		RBD (IIa)	+	-	preclinical	xxx	Tortorici et al. submitted
S2X333		NTD (i)	-	-	preclinical	7LXW 7LXY	28
Ly-CoV016	CB6/etesevimab	RBD (Ia)	+	-	EUA in US	7C01	64
Ly-CoV555	bamlanivimab	RBD (Ib)	+	-	EUA in US	7KMG	65,66
REGN10933	casirivimab	RBD (Ia)	+	-	EUA in US	6XDG	6,8
REGN10987	imdevimab	RBD (Ib)	+	-	EUA in US	6XDG	6,8
CT-P59	regdanvimab	RBD (Ia)	+	-	EUA in SK*	7CM4	67

*, SK, South Korea

References

- 1 Chi, X. *et al.* A neutralizing human antibody binds to the N-terminal domain of the Spike protein of SARS-CoV-2. *Science* **369**, 650-655, doi:10.1126/science.abc6952 (2020).
- 2 Walls, A. C. *et al.* Structure, Function, and Antigenicity of the SARS-CoV-2 Spike Glycoprotein. *Cell* **181**, 281-292 e286, doi:10.1016/j.cell.2020.02.058 (2020).
- 3 Piccoli, L. *et al.* Mapping Neutralizing and Immunodominant Sites on the SARS-CoV-2 Spike Receptor-Binding Domain by Structure-Guided High-Resolution Serology. *Cell* **183**, 1024-1042 e1021, doi:10.1016/j.cell.2020.09.037 (2020).
- 4 Greaney, A. J. *et al.* Comprehensive mapping of mutations to the SARS-CoV-2 receptor-binding domain that affect recognition by polyclonal human serum antibodies. *bioRxiv*, 1-35, doi:papers3://publication/doi/10.1101/2020.12.31.425021 (2021).
- 5 Tortorici, M. A. *et al.* Ultrapotent human antibodies protect against SARS-CoV-2 challenge via multiple mechanisms. *Science* **370**, 950-957, doi:10.1126/science.abe3354 (2020).
- 6 Hansen, J. *et al.* Studies in humanized mice and convalescent humans yield a SARS-CoV-2 antibody cocktail. *Science* **369**, 1010-1014, doi:10.1126/science.abd0827 (2020).
- 7 Chen, P. *et al.* SARS-CoV-2 Neutralizing Antibody LY-CoV555 in Outpatients with Covid-19. *N Engl J Med* **384**, 229-237, doi:10.1056/NEJMoa2029849 (2021).
- 8 Weinreich, D. M. *et al.* REGN-COV2, a Neutralizing Antibody Cocktail, in Outpatients with Covid-19. *N Engl J Med* **384**, 238-251, doi:10.1056/NEJMoa2035002 (2021).
- 9 Crawford, K. H. D. *et al.* Protocol and Reagents for Pseudotyping Lentiviral Particles with SARS-CoV-2 Spike Protein for Neutralization Assays. *Viruses* **12**, doi:10.3390/v12050513 (2020).
- 10 Hikmet, F. *et al.* The protein expression profile of ACE2 in human tissues. *Mol Syst Biol* **16**, e9610, doi:10.15252/msb.20209610 (2020).
- 11 Hou, Y. J. *et al.* SARS-CoV-2 Reverse Genetics Reveals a Variable Infection Gradient in the Respiratory Tract. *Cell* **182**, 429-446 e414, doi:10.1016/j.cell.2020.05.042 (2020).
- 12 Zou, X. *et al.* Single-cell RNA-seq data analysis on the receptor ACE2 expression reveals the potential risk of different human organs vulnerable to 2019-nCoV infection. *Front Med* **14**, 185-192, doi:10.1007/s11684-020-0754-0 (2020).
- 13 Gustine, J. N. & Jones, D. Immunopathology of Hyperinflammation in COVID-19. *Am J Pathol* **191**, 4-17, doi:10.1016/j.ajpath.2020.08.009 (2021).
- 14 Amraie, R. *et al.* CD209L/L-SIGN and CD209/DC-SIGN act as receptors for SARS-CoV-2 and are differentially expressed in lung and kidney epithelial and endothelial cells. *bioRxiv* **182**, 436-418, doi:papers3://publication/doi/10.1101/2020.06.22.165803 (2020).
- 15 Soh, W. T. *et al.* The N-terminal domain of spike glycoprotein mediates SARS-CoV-2 infection by associating with L-SIGN and DC-SIGN. *bioRxiv*, 1-30, doi:papers3://publication/doi/10.1101/2020.11.05.369264 (2020).
- 16 Wang, K. *et al.* CD147-spike protein is a novel route for SARS-CoV-2 infection to host cells. *Signal Transduct Target Ther* **5**, 283, doi:10.1038/s41392-020-00426-x (2020).

- 17 Cantuti-Castelvetri, L. *et al.* Neuropilin-1 facilitates SARS-CoV-2 cell entry and infectivity. *Science* **370**, 856-860, doi:10.1126/science.abd2985 (2020).
- 18 Clausen, T. M. *et al.* SARS-CoV-2 Infection Depends on Cellular Heparan Sulfate and ACE2. *Cell*, 1-31, doi:papers3://publication/doi/10.1016/j.cell.2020.09.033 (2020).
- 19 Thépaut, M. *et al.* DC/L-SIGN recognition of spike glycoprotein promotes SARS-CoV-2 trans-infection and can be inhibited by a glycomimetic antagonist. doi:10.1101/2020.08.09.242917 (2020).
- 20 Izquierdo-Useros, N. *et al.* Siglec-1 is a novel dendritic cell receptor that mediates HIV-1 trans-infection through recognition of viral membrane gangliosides. *PLoS Biol* **10**, e1001448, doi:10.1371/journal.pbio.1001448 (2012).
- 21 Travaglini, K. J. *et al.* A molecular cell atlas of the human lung from single-cell RNA sequencing. *Nature* **587**, 619-625, doi:10.1038/s41586-020-2922-4 (2020).
- 22 Ren, X. *et al.* COVID-19 immune features revealed by a large-scale single cell transcriptome atlas. *Cell*, doi:10.1016/j.cell.2021.01.053 (2021).
- 23 Liao, M. *et al.* Single-cell landscape of bronchoalveolar immune cells in patients with COVID-19. *Nat Med* **26**, 842-844, doi:10.1038/s41591-020-0901-9 (2020).
- 24 Rappazzo, C. G. *et al.* Broad and potent activity against SARS-like viruses by an engineered human monoclonal antibody. *Science* **371**, 823-829, doi:10.1126/science.abf4830 (2021).
- 25 Suryadevara, N. *et al.* Neutralizing and protective human monoclonal antibodies recognizing the N-terminal domain of the SARS-CoV-2 spike protein. *Cell*, doi:10.1016/j.cell.2021.03.029 (2021).
- 26 Chen, R. E. *et al.* Resistance of SARS-CoV-2 variants to neutralization by monoclonal and serum-derived polyclonal antibodies. *Nat Med*, doi:10.1038/s41591-021-01294-w (2021).
- 27 Pinto, D. *et al.* Cross-neutralization of SARS-CoV-2 by a human monoclonal SARS-CoV antibody. *Nature* **583**, 290-295, doi:10.1038/s41586-020-2349-y (2020).
- 28 McCallum, M. *et al.* N-terminal domain antigenic mapping reveals a site of vulnerability for SARS-CoV-2. *Cell*, doi:10.1016/j.cell.2021.03.028 (2021).
- 29 Chan, J. F. *et al.* Simulation of the Clinical and Pathological Manifestations of Coronavirus Disease 2019 (COVID-19) in a Golden Syrian Hamster Model: Implications for Disease Pathogenesis and Transmissibility. *Clin Infect Dis* **71**, 2428-2446, doi:10.1093/cid/ciaa325 (2020).
- 30 Gottlieb, R. L. *et al.* Effect of Bamlanivimab as Monotherapy or in Combination With Etesevimab on Viral Load in Patients With Mild to Moderate COVID-19: A Randomized Clinical Trial. *JAMA* **325**, 632-644, doi:10.1001/jama.2021.0202 (2021).
- 31 Winkler, E. S. *et al.* Human neutralizing antibodies against SARS-CoV-2 require intact Fc effector functions and monocytes for optimal therapeutic protection. *bioRxiv*, 1-53, doi:10.1101/2020.12.28.424554 (2020).
- 32 Baum, A. *et al.* REGN-COV2 antibodies prevent and treat SARS-CoV-2 infection in rhesus macaques and hamsters. *Science* **370**, 1110-1115, doi:10.1126/science.abe2402 (2020).
- 33 Rogers, T. F. *et al.* Isolation of potent SARS-CoV-2 neutralizing antibodies and protection from disease in a small animal model. *Science* **369**, 956-963, doi:10.1126/science.abc7520 (2020).
- 34 Buchrieser, J. *et al.* Syncytia formation by SARS-CoV-2-infected cells. *EMBO J* **39**, e106267, doi:10.15252/emboj.2020106267 (2020).

- 35 Bussani, R. *et al.* Persistence of viral RNA, pneumocyte syncytia and thrombosis are hallmarks of advanced COVID-19 pathology. *EBioMedicine* **61**, 103104, doi:10.1016/j.ebiom.2020.103104 (2020).
- 36 Walls, A. C. *et al.* Unexpected Receptor Functional Mimicry Elucidates Activation of Coronavirus Fusion. *Cell* **176**, 1026-1039 e1015, doi:10.1016/j.cell.2018.12.028 (2019).
- 37 Wan, Y. *et al.* Molecular Mechanism for Antibody-Dependent Enhancement of Coronavirus Entry. *The Journal of Virology* **94**, 69-15, doi:papers3://publication/doi/10.1128/JVI.02015-19 (2020).
- 38 Blanco-Melo, D. *et al.* Imbalanced Host Response to SARS-CoV-2 Drives Development of COVID-19. *Cell* **181**, 1036-1045 e1039, doi:10.1016/j.cell.2020.04.026 (2020).
- 39 Ziegler, C. G. K. *et al.* SARS-CoV-2 Receptor ACE2 Is an Interferon-Stimulated Gene in Human Airway Epithelial Cells and Is Detected in Specific Cell Subsets across Tissues. *Cell* **181**, 1016-1035 e1019, doi:10.1016/j.cell.2020.04.035 (2020).
- 40 Onabajo, O. O. *et al.* Interferons and viruses induce a novel truncated ACE2 isoform and not the full-length SARS-CoV-2 receptor. *Nat Genet* **52**, 1283-1293, doi:10.1038/s41588-020-00731-9 (2020).
- 41 Blume, C. *et al.* A novel isoform of ACE2 is expressed in human nasal and bronchial respiratory epithelia and is upregulated in response to RNA respiratory virus infection. *bioRxiv*, doi:10.1101/2020.07.31.230870 (2020).
- 42 Chang, Y. C. & Nizet, V. Siglecs at the Host-Pathogen Interface. *Adv Exp Med Biol* **1204**, 197-214, doi:10.1007/978-981-15-1580-4_8 (2020).
- 43 Cathcart, A. L. *et al.* The dual function monoclonal antibodies VIR-7831 and VIR-7832 demonstrate potent in vitro and in vivo activity against SARS-CoV-2. *bioRxiv*, doi:10.1101/2021.03.09.434607 (2021).
- 44 Xu, Z. *et al.* Pathological findings of COVID-19 associated with acute respiratory distress syndrome. *The Lancet Respiratory Medicine* **8**, 420-422, doi:10.1016/s2213-2600(20)30076-x (2020).
- 45 Tian, S. *et al.* Pulmonary Pathology of Early-Phase 2019 Novel Coronavirus (COVID-19) Pneumonia in Two Patients With Lung Cancer. *J Thorac Oncol* **15**, 700-704, doi:10.1016/j.jtho.2020.02.010 (2020).
- 46 Franks, T. J. *et al.* Lung pathology of severe acute respiratory syndrome (SARS): a study of 8 autopsy cases from Singapore. *Hum Pathol* **34**, 743-748, doi:10.1016/s0046-8177(03)00367-8 (2003).
- 47 Cohen, M. S. Monoclonal Antibodies to Disrupt Progression of Early Covid-19 Infection. *N Engl J Med* **384**, 289-291, doi:10.1056/NEJMe2034495 (2021).
- 48 Suloway, C. *et al.* Automated molecular microscopy: the new Legimon system. *J Struct Biol* **151**, 41-60, doi:10.1016/j.jsb.2005.03.010 (2005).
- 49 Hsieh, C. L. *et al.* Structure-based design of prefusion-stabilized SARS-CoV-2 spikes. *Science* **369**, 1501-1505, doi:10.1126/science.abd0826 (2020).
- 50 Tegunov, D. & Cramer, P. Real-time cryo-electron microscopy data preprocessing with Warp. *Nat Methods* **16**, 1146-1152, doi:10.1038/s41592-019-0580-y (2019).
- 51 Punjani, A., Rubinstein, J. L., Fleet, D. J. & Brubaker, M. A. cryoSPARC: algorithms for rapid unsupervised cryo-EM structure determination. *Nat Methods* **14**, 290-296, doi:10.1038/nmeth.4169 (2017).
- 52 Zivanov, J. *et al.* New tools for automated high-resolution cryo-EM structure determination in RELION-3. *Elife* **7**, doi:10.7554/eLife.42166 (2018).

- 53 Punjani, A., Zhang, H. & Fleet, D. J. Non-uniform refinement: adaptive regularization improves single-particle cryo-EM reconstruction. *Nat Methods* **17**, 1214-1221, doi:10.1038/s41592-020-00990-8 (2020).
- 54 Zivanov, J., Nakane, T. & Scheres, S. H. W. A Bayesian approach to beam-induced motion correction in cryo-EM single-particle analysis. *IUCrJ* **6**, 5-17, doi:10.1107/S205225251801463X (2019).
- 55 Pettersen, E. F. *et al.* UCSF ChimeraX: Structure visualization for researchers, educators, and developers. *Protein Sci* **30**, 70-82, doi:10.1002/pro.3943 (2021).
- 56 Casanal, A., Lohkamp, B. & Emsley, P. Current developments in Coot for macromolecular model building of Electron Cryo-microscopy and Crystallographic Data. *Protein Sci* **29**, 1069-1078, doi:10.1002/pro.3791 (2020).
- 57 Corti, D. *et al.* A neutralizing antibody selected from plasma cells that binds to group 1 and group 2 influenza A hemagglutinins. *Science* **333**, 850-856, doi:10.1126/science.1205669 (2011).
- 58 Tortorici, M. A. *et al.* Ultrapotent human antibodies protect against SARS-CoV-2 challenge via multiple mechanisms. *Science*, doi:10.1126/science.abe3354 (2020).
- 59 Boudewijns, R. *et al.* STAT2 signaling restricts viral dissemination but drives severe pneumonia in SARS-CoV-2 infected hamsters. *Nat Commun* **11**, 5838, doi:10.1038/s41467-020-19684-y (2020).
- 60 Reed, L. J. & Muench, H. A SIMPLE METHOD OF ESTIMATING FIFTY PER CENT ENDPOINTS¹². *American Journal of Epidemiology* **27**, 493-497, doi:10.1093/oxfordjournals.aje.a118408 (1938).
- 61 Sanchez-Felipe, L. *et al.* A single-dose live-attenuated YF17D-vectored SARS-CoV-2 vaccine candidate. *Nature* **590**, 320-325, doi:10.1038/s41586-020-3035-9 (2021).
- 62 Alexandersen, S., Chamings, A. & Bhatta, T. R. SARS-CoV-2 genomic and subgenomic RNAs in diagnostic samples are not an indicator of active replication. *Nat Commun* **11**, 6059, doi:10.1038/s41467-020-19883-7 (2020).
- 63 Wu, F. *et al.* A new coronavirus associated with human respiratory disease in China. *Nature* **579**, 265-269, doi:10.1038/s41586-020-2008-3 (2020).
- 64 Shi, R. *et al.* A human neutralizing antibody targets the receptor-binding site of SARS-CoV-2. *Nature* **584**, 120-124, doi:10.1038/s41586-020-2381-y (2020).
- 65 Jones, B. E. *et al.* LY-CoV555, a rapidly isolated potent neutralizing antibody, provides protection in a non-human primate model of SARS-CoV-2 infection. *bioRxiv* **395**, 497-429, doi:papers3://publication/doi/10.1101/2020.09.30.318972 (2020).
- 66 Group, A.-T. L.-C. S. *et al.* A Neutralizing Monoclonal Antibody for Hospitalized Patients with Covid-19. *N Engl J Med* **384**, 905-914, doi:10.1056/NEJMoa2033130 (2021).
- 67 Kim, C. *et al.* A therapeutic neutralizing antibody targeting receptor binding domain of SARS-CoV-2 spike protein. *Nat Commun* **12**, 288, doi:10.1038/s41467-020-20602-5 (2021).